Anomalous diffusion and nonergodicity for heterogeneous diffusion processes with fractional Gaussian noise

Wei Wang,[1,2] Andrey G. Cherstvy [○],[2] Xianbin Liu,[1] and Ralf Metzler [○][2,*]

[1]*College of Aerospace Engineering, Nanjing University of Aeronautics and Astronautics, 210016 Nanjing, China*

[2]*Institute for Physics & Astronomy, University of Potsdam, 14476 Potsdam-Golm, Germany*

Heterogeneous diffusion processes (HDPs) feature a space-dependent diffusivity of the form $D(x) = D_0|x|^\alpha$. Such processes yield anomalous diffusion and weak ergodicity breaking, the asymptotic disparity between ensemble and time averaged observables, such as the mean-squared displacement. Fractional Brownian motion (FBM) with its long-range correlated yet Gaussian increments gives rise to anomalous and ergodic diffusion. Here, we study a combined model of HDPs and FBM to describe the particle dynamics in complex systems with position-dependent diffusivity driven by fractional Gaussian noise. This type of motion is, *inter alia*, relevant for tracer-particle diffusion in biological cells or heterogeneous complex fluids. We show that the long-time scaling behavior predicted theoretically and by simulations for the ensemble- and time-averaged mean-squared displacements couple the scaling exponents α of HDPs and the Hurst exponent H of FBM in a characteristic way. Our analysis of the simulated data in terms of the rescaled variable $y \sim |x|^{1/(2/(2-\alpha))}/t^H$ coupling particle position x and time t yields a simple, Gaussian probability density function (PDF), $P_{\text{HDP-FBM}}(y) = e^{-y^2}/\sqrt{\pi}$. Its universal shape agrees well with theoretical predictions for both uni- and bimodal PDF distributions.

I. INTRODUCTION

Classical Brownian motion (BM) is characterized by two fundamental properties: the Gaussian form of its probability density function (PDF),

$$P(x,t) = \frac{1}{\sqrt{4\pi K_1 t}} \exp\left(-\frac{x^2}{4K_1 t}\right), \tag{1}$$

where K_1 is the diffusion coefficient, and the linear time dependence of the mean-squared displacement (MSD),

$$\langle x^2(t) \rangle = 2K_1 t. \tag{2}$$

Hereafter we consider a one-dimensional setting. Despite the universal nature of the Gaussian PDF (1), in many real systems the fundamental properties (1) and (2) are violated. Particularly, anomalous diffusion of the non-Fickian power-law form [1–14]

$$\langle x^2(t) \rangle = 2K_\gamma t^\gamma \tag{3}$$

has been widely observed across many disciplines. Here K_γ is the generalized diffusion coefficient of physical dimension $\text{m}^2/\text{s}^\gamma$ and γ is the anomalous diffusion exponent. A process characterized by the MSD (3) is called subdiffusive for $0 < \gamma < 1$ and superdiffusive for $1 < \gamma < 2$. The range $\gamma > 2$ is sometimes referred to as hyperdiffusive. For $\gamma = 1$ we recover normal (Fickian) BM, while ballistic motion corresponds to $\gamma = 2$.

Experimentally, subdiffusion was observed for submicron tracers in the crowded cytoplasm of biological cells [15–20], in artificially crowded liquids [21–23], and for motion of proteins embedded in the membranes of living cells [24–27]. Subdiffusion is also seen in extensive simulations studies, for instance, of lipid bilayer membranes [13,28–30] and relative diffusion in proteins [31]. Superdiffusion fuelled by molecular motors was observed in various types of biological cells for both introduced and endogenous tracers including virus particles [16,17,32–35].

In lieu of the universal Gaussian law (1) governing BM, anomalous diffusion may emerge from a variety of stochastic processes [1–14]. Among these is the famed Scher-Montroll-Weiss continuous-time random walk (CTRW) characterized by independent of coupled probability densities of the single-jump lengths and waiting times [36–38]. When the waiting times are scale-free power laws, this process describes subdiffusion, as, e.g., observed for the short-time motion of lipid granules in yeast cells [19], diffusion of potassium channels in cell membranes [25], or the relative dynamics in single proteins [31]. Superdiffusive versions of CTRW, so-called Lévy walks [8], were, e.g., observed for active molecular-motor-driven motion in biological cells [34,35]. Another prominent model for anomalous diffusion is the random walk on fractal structures [3], e.g., as observed as ingredient of potassium channel diffusion in cell membranes [25]. We also mention scaled BM (SBM) [39] yielding anomalous diffusion due to a power-law time dependence of the diffusion coefficient. This type of dynamics is, e.g., systemic for diffusion in granular gases in the homogeneous cooling phase [40].

Two important classes of anomalous diffusion are long-range power-law correlated fractional Brownian motion (FBM) and heterogeneous diffusion processes (HDPs) based on power-law scaling forms of the diffusivity as function of distance. These two processes are at the core of this study and will be discussed along with concrete applications in the

———
*rmetzler@uni-potsdam.de

next section. The main goal is to quantify the behavior of the compound HDP-FBM process.

In fact, the need to combine more than a single stochastic process in order to faithfully describe measured data does not come as a surprise, given the highly complex environment of, e.g., living biological cells and their constituents or crowded and structured liquids. For instance, the motion of lipid granules in yeast cells [19] was shown to follow scale-free waiting-time-dominated subdiffusion at short and FBM at long times. The potassium channel motion in membranes [25] and the diffusion of insulin granules in cells [20] showed that clear signatures of the simultaneous action of scale-free power-law waiting times and, respectively, a fractal geometry of the support and FBM-like correlations conspire the data.

The paper is structured as follows. In Secs. II A and II B we introduce FBM and HDPs, respectively, and discuss their relevance to actual systems. We overview some details of simulations in Sec. III and present the main results of the theoretical analysis and simulations for the HDP-FBM model in Sec. IV. The discussion and conclusions are provided in Sec. V. We discuss the shape similarities of the PDF in Appendix A and present additional figures in Appendix B.

II. FBM AND HDPS

A. FBM

A widely used class of anomalous-diffusion models is based on correlated yet stationary noise. For example, the famed model of FBM [41–45] obeys the overdamped Langevin equation

$$\frac{dx(t)}{dt} = \xi_H(t), \tag{4}$$

where the correlation function of the (external) fractional Gaussian noise $\xi_H(t)$ for $t_1 \neq t_2$ is given by

$$\langle \xi_H(t_1)\xi_H(t_2)\rangle \simeq K_{2H}2H(2H-1) \times |t_1-t_2|^{2H-2}. \tag{5}$$

Here $H = \gamma/2$ is the Hurst exponent. In contrast to standard BM driven by white Gaussian noise, for FBM the increments feature strong long-range correlations (non-Markovian). Persistent (positive) and antipersistent (negative) correlations, in Mandelbrot's terms [43], lead to superdiffusion and subdiffusion, respectively. Such long-range power-law correlations are prototypical for viscoelastic systems [19,22,23,29,33,46–48].

The PDF for FBM is Gaussian,

$$P_{\text{FBM}}(x,t) = \frac{1}{\sqrt{4\pi K_{2H}t^{2H}}} \exp\left(-\frac{x^2}{4K_{2H}t^{2H}}\right), \tag{6}$$

for the initial Dirac-δ condition

$$P(x,t=0) = \delta(x) \tag{7}$$

and natural boundary conditions $P(|x| \to \infty, t) = 0$. The PDF (6) satisfies the generalized diffusion equation [49]

$$\frac{\partial}{\partial t}P_{\text{FBM}}(x,t) = 2Ht^{2H-1}K_{2H}\frac{\partial^2}{\partial x^2}P_{\text{FBM}}(x,t) \tag{8}$$

and yields the MSD,

$$\langle x^2_{\text{FBM}}(t)\rangle = \int_{-\infty}^{\infty} x^2 P_{\text{FBM}}(x,t)dx = 2K_{2H}t^{2H}. \tag{9}$$

Note that Eq. (8) cannot be simply used for FBM in the presence of reflecting or absorbing boundaries [39,50,51].

In contrast to the MSD (9) in the sense of ensemble averaging, many experiments based on single-particle tracking or simulations of individual particle trajectories are evaluated in terms of the time-averaged MSD (TAMSD) [6,7]

$$\overline{\delta^2(\Delta)} = \frac{1}{T-\Delta}\int_0^{T-\Delta} [x(t+\Delta)-x(t)]^2 dt. \tag{10}$$

For BM, the TAMSD (10) converges to the MSD for long measurement times T on the single-trajectory level,

$$\lim_{\Delta/T \to 0} \overline{\delta^2(\Delta)} = \langle x^2(\Delta)\rangle. \tag{11}$$

In the Boltzmann-Khinchin sense, this is an ergodic behavior; Bouchaud called a system weakly nonergodic when this equivalence is violated [52]. This definition is practically important for applications of stochastic models but is less stringent than definitions of nonergodicity used in ergodic theory [53]. An overview of weakly nonergodic behavior of various stochastic processes can be found in Refs. [6,11].

The mean TAMSD for an ensemble of N independent TAMSD measurements at a given lag time Δ and measurement time T is computed as

$$\langle \overline{\delta^2(\Delta)}\rangle = \frac{1}{N}\sum_{i=1}^{N} \overline{\delta_i^2(\Delta)}. \tag{12}$$

For any finite Δ and T each trajectory exhibits certain variations of $\overline{\delta^2(\Delta)}$. This amplitude variation between the TAMSDs (10) of individual trajectories around their mean (12) is quantified by the ergodicity breaking parameter [6,11,45]

$$\text{EB}(\Delta) = \langle \xi(\Delta)^2\rangle - 1, \tag{13}$$

where $\xi(\Delta) = \overline{\delta^2(\Delta)}/\langle \overline{\delta^2(\Delta)}\rangle$ such that $\langle \xi \rangle = 1$. For standard BM in the continuous-time limit one finds the convergence $\lim_{\Delta/T \to 0}\text{EB}_{\text{BM}}(\Delta) = 4\Delta/(3T)$ to ergodic behavior, with full reproducibility of long trajectories, $\lim_{T\to\infty}\text{EB}_{\text{BM}}(\Delta)=0$ [45,54,55].

For FBM the ergodicity condition (11) holds,

$$\langle x^2_{\text{FBM}}(\Delta)\rangle = \langle \overline{\delta^2_{\text{FBM}}(\Delta)}\rangle = 2K_{2H}\Delta^{2H}. \tag{14}$$

The ergodic properties of FBM are quantified in terms of EB in Refs. [45,56]. Note that for EB of FBM the implications of external confinement [57,58] as well as modifications due to random-diffusivity effects (see Refs. [59–61]) and finiteness of the step size [62] were examined as well. A combined model of FBM and CTRWs was recently applied to describe the nonergodic dynamics in heterogeneous media with random characteristic length scales [63].

Diverse mathematical models of FBM-based anomalous diffusion have been successfully applied to describe the dynamics in a number of physical and biological systems. The list includes the dynamics of various tracers in artificially crowded solutions and in the cell cytoplasm, e.g., the diffusion of individual labeled mRNA molecules in living *Escherichia coli* cells [64], long-time diffusion of lipid granules in living fission-yeast cells [19], telomere diffusion in the nuclei of human cancer U2OS cells [48,65], fluorescence-correlation-spectroscopy-based analysis of crowded dextran

solutions [22], etc. The effect of localization errors on the degree of MSD anomaly for FBM-based trajectories was examined recently [66].

Moreover, the diffusive motion based on the overdamped fractional Langevin equation (a thermal process closely related to FBM) was shown to describe the dynamics of the lipid and cholesterol molecules in lipid bilayers [29] and subdiffusive motion of chromosomal loci in the bacterial cytoplasm [47]. A combination of ergodic FBM and non-ergodic CTRWs [67] was shown to be consistent with the motion of insulin granules in human cells [20]. The dynamics of tracked chromosomal loci in yeast was shown to be subdiffusive and consistent with FBM [68] (after accounting for particle-localization errors). Chromosomal loci in bacterial-cells were demonstrated to diffuse similar to fractional-Langevin-equation-driven motion [69]. A feasible physical rationale for subdiffusive dynamics based on fractional Langevin equation and FBM-type dynamics in many of these systems are the viscoelastic properties of the (often highly crowded) environments inside biological cells [70]. We finally mention that FBM-based models were applied to generalize aspects of gene regulation [71,72] and chemical reactions [73,74] in Refs. [75,76].

B. HDPs

Recently, we proposed the model of HDPs [77–82], a class of stochastic processes driven by standard Gaussian white noise $\xi(t)$ with zero mean $\langle \xi(t) \rangle = 0$ and pair correlation,

$$\langle \xi(t_1)\xi(t_2) \rangle = \delta(t_1 - t_2), \tag{15}$$

in media with a position-dependent diffusivity (or state-dependent diffusion [83]). In most situations, a power-law variation of the diffusion coefficient is prescribed for such (generally nonequilibrium) physical systems, namely

$$D(x) = D_0 |x|^\alpha. \tag{16}$$

Here the physical dimensions of D_0 are $[D_0] = \mathrm{m}^{2-\alpha}/\mathrm{s}$. In fact, a diffusion equation with $D(x) \propto |x|^{4/3}$ was first formulated by Richardson to study atmospheric turbulence [84], see also Refs. [85–88]. Our major advance regarding this nonergodic system was the analytical and numerical analysis of the MSD and mean TAMSD [77–82], as well as the physical characteristics of the particle dispersion for general scaling exponent α.

Systems with exponentially and logarithmically varying diffusivities [78] were examined as well based on their MSD and TAMSD. We also considered HDPs with external hard-wall confinement and ageing [80]. Modifications of HDPs with Lévy noise [89], in potential landscapes [90], in comb or fractal structures [91] (see also Ref. [92]), in different stochastic interpretations and for higher moments [93], as well as with respect to infinite ergodic theory [94] were recently developed. Effects of $D(x)$ on diffusion in periodic channels were recently studied as well [95]. Quantum BM for inhomogeneous diffusion was also investigated [96,97].

For HDPs with $D(x) = D_0 |x|^\alpha$ the standard overdamped multiplicative-noise Langevin equation

$$\frac{dx(t)}{dt} = \sqrt{2D(x)}\,\xi(t) \tag{17}$$

is solved. In the Stratonovich representation—see below and Sec. V for a discussion of other conventions [98,99]—the exact solution for the MSD of HDPs is [77]

$$\langle x_{\mathrm{HDP}}^2(t) \rangle = \int_{-\infty}^{\infty} x^2 P_{\mathrm{HDP}}(x,t)\,dx = C_p t^p. \tag{18}$$

Here the prefactor reads

$$C_p = \frac{\Gamma(p+1/2)}{\pi^{1/2}} \left(\frac{2}{p}\right)^{2p} D_0^p \tag{19}$$

in terms of the Γ function, and the scaling exponent is

$$p = 2/(2 - \alpha). \tag{20}$$

HDPs are superdiffusive for $2 > \alpha > 0$ (or $p > 1$) and subdiffusive for $\alpha < 0$ (i.e., $0 < p < 1$).

The PDF of the particle displacements after time t starting from the initial δ-condition (7) is given by the modified stretched or compressed Gaussian function

$$P_{\mathrm{HDP}}(x,t) = \frac{|x|^{1/p-1}}{\sqrt{4\pi D_0 t}} \exp\left[-\frac{|x|^{2/p}}{(2/p)^2 D_0 t}\right] \tag{21}$$

satisfying the symmetrized [100] diffusion equation (see Ref. [77])

$$\frac{\partial}{\partial t}P_{\mathrm{HDP}}(x,t) = \frac{\partial}{\partial x}\left\{\sqrt{D(x)}\frac{\partial}{\partial x}[\sqrt{D(x)}P_{\mathrm{HDP}}(x,t)]\right\}. \tag{22}$$

For $\alpha < 0$ (or $p < 1$) the PDF (21) has a bimodal shape with two symmetric peaks spreading with time, while for $\alpha > 0$ (or $p > 1$) PDF $P_{\mathrm{HDP}}(x,t)$ features a single cusp at $x = 0$ with the PDF tails spreading with time. The cusp corresponds to particle localization in the region of low diffusivity near $x = 0$ (see Fig. 1 of Ref. [77]).

While above we used the Stratonovich interpretation of the multiplicate-noise stochastic equation (17), we note that other stochastic interpretations for HDPs were shown [93] to lead to different prefactors C_p and also differen PDF shapes, but leave the scaling (18) for the MSD unaltered. Using the generalized notation

$$\frac{\partial}{\partial t}P_{\mathrm{HDP}}(x,t) = \frac{\partial}{\partial x}\left([D(x)]^\varkappa \frac{\partial}{\partial x}\big\{[D(x)]^{1-\varkappa} P_{\mathrm{HDP}}(x,t)\big\}\right) \tag{23}$$

we mention explicitly the Itô (prepoint, $\varkappa = 0$) [101], Fisk-Stratonovich (middle point, $\varkappa = 1/2$) [102,103], and Hänggi-Klimontovich (postpoint, $\varkappa = 1$, also called "isothermal" or "kinetic") [104,105] conventions (see Refs. [83,100,105–110] for more details). As we mainly have nonequilibrium systems in mind—such as living biological cells or actively moving particles in heterogeneous environments—we are not confined to thermalization conditions and use the convenient Stratonovich convention.

The TAMSD for HDPs remains strictly linear in lag time for all diffusivity exponents α, namely [77]

$$\overline{\delta_{\mathrm{HDP}}^2(\Delta)} = C_p \frac{\Delta}{T^{1-p}}, \tag{24}$$

giving rise to the conclusion that HDPs are weakly nonergodic [77],

$$\frac{\left\langle \overline{\delta_{\mathrm{HDP}}^2(\Delta)} \right\rangle}{\left\langle x_{\mathrm{HDP}}^2(\Delta) \right\rangle} = \left(\frac{\Delta}{T} \right)^{1-p}. \tag{25}$$

Diverse physical systems exhibit features of heterogeneous diffusion. For instance, the diffusion equation in atmospheric diffusion of substances with height-dependent diffusion coefficient and wind velocity of the form (16) was considered long ago (see Refs. [111,112] and the historical overview [112]). Note that exponentially decaying diffusivities $D(x) \propto e^{-\kappa x}$ were applied to the description of impurity-concentration profiles in irradiation-enhanced diffusion [113] and to bombardment-enhanced diffusion [114], while $D(x) \propto e^{\kappa/x}$ was employed for diffusion near nonequilibrium grain boundaries [115]. Classical examples of power-law $D(x)$ (16) include hydrodynamic-mediated tracer diffusion near walls and the spreading dynamics in confined geometries [116–120].

Water and contaminant diffusion in porous heterogeneous and fractured geological media often involves space-dependent and anisotropic diffusivity profiles [121–123] (see also Ref. [124])—heterogeneous media with stratified and randomly distributed diffusivity were also considered. We emphasize here the emergence of bimodal concentration profiles for superdiffusive propagation of passive tracers in heterogeneous media [122]. Certain heterogeneous systems feature different $D(x)$-trends on different spatial scales. Recent examples in a more general context of $D(x)$ systems related to cell biophysics include the diffusion of tracers in heterogeneously crowded cytoplasm of living cells [125–127], obstructed tracer diffusion in heterogeneously crowded *in silico* environments mimicking the cell cytoplasm [128], protein diffusion on heterogeneous landscapes on DNA molecules [129,130], etc. In the context of transport in periodic channels heterogeneous diffusion was shown to significantly alter the transport efficiency [95]. Finally, heterogeneity on the tissue level was shown to influence cardiac electrical propagation [131].

For a generalized HDP-SBM scenario, with position- and time-dependent diffusivity of the form

$$D(x,t) \sim |x|^\alpha t^\beta \tag{26}$$

we obtained [82] that the MSD and mean TAMSD scaling relations (18) and (24) remain valid with the intuitive renomalization

$$p \to p(1+\beta). \tag{27}$$

This scaling exponent is the product of the original HDP exponent (20) and the respective exponent of SBM [39,132]. The same renormalization was shown to be true for the aged TAMSD, defined as [6,11]

$$\overline{\delta_a^2(\Delta)} = \frac{1}{T-\Delta} \int_{t_a}^{t_a+T-\Delta} [x(t+\Delta) - x(t)]^2 dt, \tag{28}$$

with the ratio of the aged to the nonaged TAMSDs [82]

$$\Lambda_{p,\beta}\left(\frac{t_a}{T} \right) = \frac{\left\langle \overline{\delta_a^2(\Delta)} \right\rangle}{\left\langle \overline{\delta^2(\Delta)} \right\rangle} \sim \left(1 + \frac{t_a}{T} \right)^{p(1+\beta)} - \left(\frac{t_a}{T} \right)^{p(1+\beta)}. \tag{29}$$

Remarkably, an identical ageing form was observed for CTRWs [133,134] and pure SBM [40,135]. One can anticipate that for the HDP-FBM model a similar renormalization of the scaling exponents in the MSD and mean TAMSD will be valid, as we indeed show below.

III. SIMULATION METHODS FOR THE HDP-FBM PROCESS

In the current study, we combine the model of HDPs with FBM noise and solve the stochastic differential multiplicative-noise equation

$$\frac{dx(t)}{dt} = \sqrt{2D(x)}\xi_H(t), \tag{30}$$

with the noise correlator (5) (where ξ_H is normalized below, as compared to Eq. (4), by the dimensions of $1/\sqrt{D}$ being $\sqrt{\text{time}}/\text{length}$ that yields the units $[\xi_H] = 1/\sqrt{s}$, where s denotes seconds) and the space-dependent diffusivity (16). We split the consideration of the HDP-FBM model into four scenarios: (i) superdiffusive HDPs and subdiffusive FBM ($\alpha > 0$ and $0 < H < 1/2$), (ii) superdiffusive HDPs and superdiffusive FBM ($\alpha > 0$ and $1 > H > 1/2$), (iii) subdiffusive HDPs and superdiffusive FBM ($\alpha < 0$ and $1 > H > 1/2$), and (iv) subdiffusive HDPs and subdiffusive FBM ($\alpha < 0$ and $0 < H < 1/2$). These four regimes are shown in Fig. 1.

For $\alpha > 0$ we simulate the original diffusivity $D(x) = D_0|x|^\alpha$ (without any modification), while at $\alpha < 0$ to avoid excessive localization of the particles near the origin we "regularize" the diverging diffusivity (16). For instance, for $D(x) = D_0/x^2$ we employ the regularized form [77]

$$D(x) = D_0 A/(A + x^2), \tag{31}$$

with $A = 0.1$ and $D_0 = 1$ fixed throughout the paper. The same procedure is employed for all the values of $\alpha < 0$. The time step used in the discretized simulation scheme for
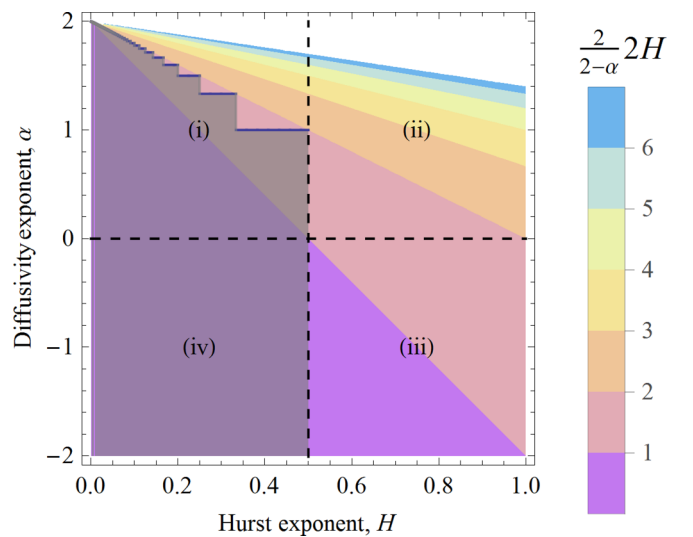

FIG. 1. Variation of the resulting MSD scaling exponent for the HDP-FBM process, see Eq. (35), in the plane of exponents H and α. The gray-shaded exclusion region defined by Eq. (34) cannot be considered within the employed Stratonovich-based simulation technique (32).

Eq. (30) is $\delta t = 10^{-2}$ for most of the results presented below (except for those in Fig. 6).

We simulate Eq. (30) effectively in the Itô representation using the algorithm and simulation code developed recently [62] and employing the conversion algorithm between the Stratonovich and Itô schemes proposed for FBM in Ref. [136]. According to this procedure, the Stratonovich version of (30) requires adding the following term to the right-hand side of the Itô form,

$$\sqrt{2D(x_i)}dB_H|_{\text{Strat}} = \sqrt{2D(x_i)}dB_H|_{\text{Itô}}$$

$$+ \sum_{m=1}^{\infty} \frac{\partial^m}{\partial x^m}[\sqrt{2D(x_{i-1})}] \frac{[\sqrt{2D(x_{i-1})}]^m(\delta t)^{(m+1)H}}{2^m m!}. \quad (32)$$

Here $B_H(t)$ denotes FBM. For $H = 1/2$ [the pure HDP (17)] we see that for $x > 0$ and $D(x) = D_0 x^\alpha$ this additional term is $D_0 \alpha x^{\alpha-1}(\delta t)/2$ (see also Eq. (3.54) in Ref. [93]). For $H > 1/2$ and small simulation time steps δt, all terms containing δt in Eq. (32) have powers higher than unity and can be neglected to leading order. Thus, in the diffusion scenarios (ii) and (iii) categorized above the Stratonovich-based simulation scheme will give the same results as the Itô-based scheme. We refer the reader to chapters 5 and 6 in Ref. [137] for stochastic and pathwise integrals for FBM, in particular for $0 < H < 1/2$.

For $H < 1/2$ the same conditions on the powers of terms $\propto \delta t^{(m+1)H}$ to be higher than unity yields that the sum in Eq. (32) should be taken at least up to the order

$$m_{\min} = \lfloor 1/H \rfloor - 1, \quad (33)$$

where $\lfloor \cdot \rfloor$ is the floor function. Computing the magnitude of the mth term in (32) and taking the derivatives, we have to assure that no divergence occurs at $x = 0$. This condition requires for the mth order of this additional term (scaling as $\propto |x|^{\alpha/2 - m + \alpha m/2}$) to have a positive exponent, in order to avoid additional renormalization of $D(x)$, as in Eq. (31). This condition yields an increasing function of m, namely $\alpha_m \geqslant 2 - 2/(m + 1)$, and the lower boundary for α_m follows from using (33) as $m = m_{\min}$. As a result, the condition for regions (i) and (iv), in which a consistent Stratonovich-based scheme can be employed is

$$\alpha \geqslant 2 - \frac{2}{\lfloor 1/H \rfloor}. \quad (34)$$

The latter restricts the region of the permitted model parameters α and H. In particular, consistent Stratonovich-based simulations are not possible for region (iv) and only possible in the restricted domain of α and H for scenario (i)—namely, outside of the shaded region of parameters in Fig. 1.

As we show below, the MSD and mean TAMSD for the combined HDP-FBM process scale, respectively, as

$$\langle x_{\text{HDP-FBM}}^2(t) \rangle = C_p t^{2Hp} \simeq t^{2H \times \frac{2}{2-\alpha}} \quad (35)$$

and

$$\langle \overline{\delta_{\text{HDP-FBM}}^2(\Delta)} \rangle = C_p \left(\frac{\Delta}{T^{1-\frac{2}{2-\alpha}}} \right)^{2H} \simeq \Delta^{2H}. \quad (36)$$

We show in Fig. 1 the variation of the MSD scaling exponent $2Hp$ in Eq. (35) in the plane of the Hurst exponent H and the $D(x)$-scaling exponent α.

IV. RESULTS FOR THE HDP-FBM PROCESS

A. MSD and TAMSD

We start by presenting the MSD as well as the magnitude and amplitude variation of the TAMSDs for scenarios (i), (ii), and (iii) in Figs. 2(a), 2(b), and 2(c). We observe that after the initial MSD relaxation from a small initial particle displacement ($x_0 = 0.01$) the MSD indeed follows the asymptotic law (35). In Fig. 2 we examine the actual particle positions, instead of the typical MSD definition $\langle [x(t) - x_0]^2 \rangle$. We note that the current $D(x)$-system has no translational invariance and, thus, the value of x_0 affects $\langle [x(t) - x_0]^2 \rangle$, making it a nonuniversal measure. The relaxation time toward this long-time MSD asymptote, naturally, depends on the actual x_0 value used in the simulations [specifically, on the deviation of x_0^2 from the initial value $\langle x(t = \delta t)^2 \rangle$] as well as on the exponents H and α. Plotting the measure of the particle displacements in terms of $\langle x(t)^2 \rangle$, rather than in the standard MSD manner, enables us to instantly identify the initial particle position that becomes important below (for instance, in Sec. IV B 2 where we vary x_0 and study the resulting PDF variations).

For the case of superdiffusive HDPs the magnitude of the TAMSD is higher than that of the MSD $\langle x^2(t) \rangle$ in the entire range of (lag) times, see Eq. (25). In Figs. 2(a) and 2(b) we show that this trend is also valid for the HDP-FBM process with superdiffusive HDPs, provided sufficiently small initial displacement x_0 of the particles. For the HDP-FBM model with superdiffusive HDPs the agreement of the results between computer simulations and theoretical predictions (35) and (36) is excellent and quantitative. The mean TAMSD follows the expected scaling dependence (36) almost in the entire range of lag times. At the last point $\Delta = T$, the MSD and mean TAMSD become equal, as they should due to the (weak) singularity in the definition of the TAMSD [6,11].

In contrast to superdiffusive HDPs, for pure subdiffusive HDPs the MSD $\langle x^2(t) \rangle$ is higher in magnitude than the mean TAMSD [77,81]. The same is true for the HDP-FBM process. Here, again, the initial particle displacement $|x_0|$ should not be chosen too small in order to avoid possible MSD-TAMSD intersection at short times during the period of MSD relaxation to the long-time asymptote, see Fig. 2(c). This figure shows that the long-time MSD asymptote from simulations agrees well with that from the theory, while for the magnitude of the mean TAMSD we detect a discrepancy. This discrepancy—present also in the analysis of the original HDPs (see Fig. 2(a) of Ref. [77])—may, in part, stem from the regularization of $D(x)$ employed in the simulations, see Eq. (31).

To check the amplitude of the MSD quantitatively, we performed computer simulations for systematically varying Hurst exponent H and restored the dependence of the prefactor C_p in Eqs. (35) and (36) for different α values versus H. These results, together with the theoretical prediction (19), are presented in Fig. 5. We find that for the HDP-FBM process the agreement of C_p with the theoretical predictions is good
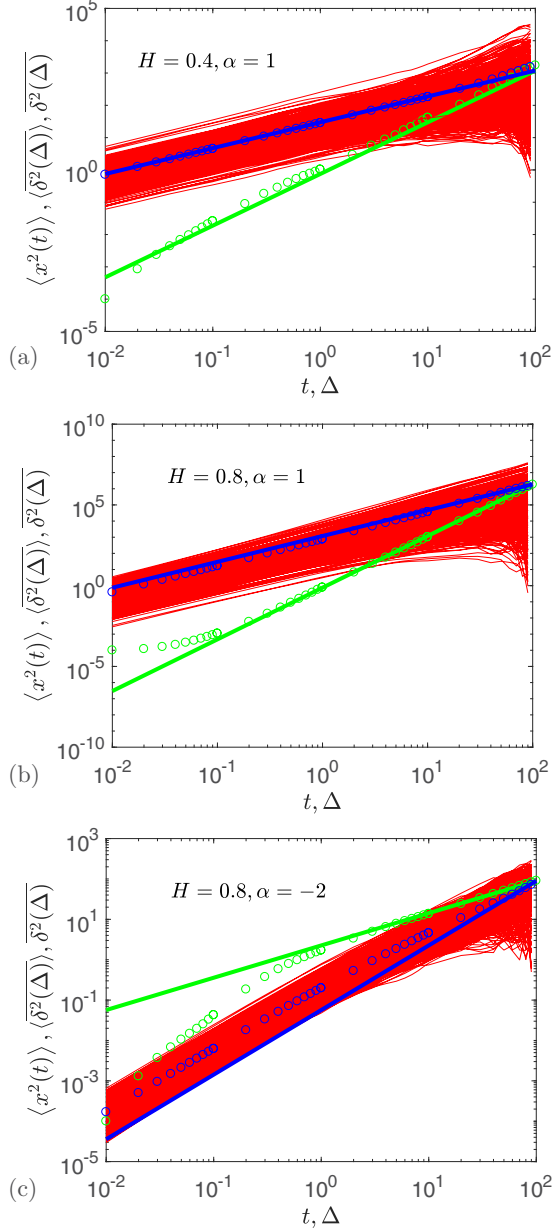
FIG. 2. MSD (in terms of $\langle x^2(t) \rangle$, green symbols and solid green curves), mean TAMSD $\langle \overline{\delta^2(\Delta)} \rangle$ (blue symbols and solid blue curves), and individual TAMSD $\overline{\delta^2(\Delta)}$ (thin red curves) for the HDP-FBM process. The MSD and TAMSD depend on their respective variables, t and Δ. The diffusion scenarios (i), (ii), and (iii) correspond to panels (a), (b), and (c) with the FBM and HDP exponents, respectively; (a) $H = 0.4$ and $\alpha = 1$, (b) $H = 0.8$ and $\alpha = 1$, and (c) $H = 0.8$ and $\alpha = -2$. Thick green and blue curves are the theoretical predictions Eqs. (35) and (36). Other parameters: the initial position of the particles is $x_0 = 10^{-2}$, the trajectory length is $T = 10^2$, the time step in simulations is $\delta t = 10^{-2}$, and averaging is performed over $N = 10^3$ time series. For all figures the noise strength is $K_{2H} = 1/2$.

particularly, for superdiffusive FBM. We also checked that MSD and TAMSD results are nearly insensitive to the value of the time step used in the simulations, see Fig. 6.

To check the dependence of the magnitude of the mean TAMSD (36) on the trajectory length T, we performed sim-

ulations for systematically varying T. In Fig. 7 we present the variation of the TAMSD at the shortest lag time, $\Delta_1 = \delta t$, namely $\langle \overline{\delta^2_{\text{HDP-FBM}}(\Delta_1)} \rangle$ versus T for the same H and α exponents as in Fig. 2. We find that the agreement of the TAMSD with respect to both scaling behavior and magnitude is particularly good for the case of superdiffusive HDPs and subdiffusive FBM [scenario (i) of the HDP-FBM model]. For superdiffusive HDPs and superdiffusive FBM some deviations in the amplitude are detected. For subdiffusive HDPs and superdiffusive FBM small discrepancies in the scaling exponent as well as in the mean-TAMSD magnitude are observed, see Fig. 7. This fact, again, may be due to the regularization of the divergence of $D(x) = D_0|x|^\alpha$ for $\alpha < 0$ near the origin, see Eq. (31), as proposed in Ref. [77]. Other choices for the regularization of $D(x)$ for $\alpha < 0$—such as capping the diffusivity at $D(|x| < \epsilon) = D(\epsilon)$—are also possible to be implemented in simulations.

Naturally, as HDPs are weakly nonergodic [77,81,82], we expect weak nonergodicity also for the HDP-FBM process. Indeed, weak ergodicity breaking is clearly demonstrated by the nonequivalence of the MSD and TAMSD for all values of the model parameters studied in Fig. 2. Using expressions (35) and (36) for the MSD and mean TAMSD, we find that the nonergodicity of pure HDPs quantified by (25) is simply rescaled for the HDP-FBM process to yield

$$\frac{\langle \overline{\delta^2_{\text{HDP-FBM}}(\Delta)} \rangle}{\langle x^2_{\text{HDP-FBM}}(\Delta) \rangle} = \left(\frac{\Delta}{T} \right)^{(1-p) \times 2H}. \tag{37}$$

The detailed evaluation of the EB parameter (13) for the HDP-FBM model, a nontrivial task due to the calculation of the fourth-order moments, is postponed for a separate study.

B. PDF

1. Symmetric distributions

The PDFs of the particle displacements—plotted for the same sets of the Hurst exponents H and diffusivity exponents α as in Fig. 2—are shown in Fig. 3. Figures 3(a), 3(b), and 3(c) of this figure correspond to the cases (i), (ii), and (iii) of the HDP-FBM model, respectively. By analogy with the parent processes of FBM and HDP, see the PDFs (6) and (21), the PDF of the HDP-FBM model for the initial condition (7) can be constructed as

$$P_{\text{HDP-FBM}}(x, t) = \frac{|x|^{1/p-1} \exp \left\{ -\left[\frac{|x|^{1/p}}{(2/p)\sqrt{D_0 t^{2H}}} \right]^2 \right\}}{\sqrt{4\pi D_0 t^{2H}}}. \tag{38}$$

This form explicitly satisfies the diffusion equation

$$\frac{\partial}{\partial t} P_{\text{HDP-FBM}}(x, t)$$

$$= 2Ht^{2H-1} \frac{\partial}{\partial x} \left\{ \sqrt{D(x)} \frac{\partial}{\partial x} [\sqrt{D(x)} P_{\text{HDP-FBM}}(x,t)] \right\}, \tag{39}$$

and is consistent with the MSD relation (35), namely

$$\langle x^2_{\text{HDP-FBM}}(t) \rangle = 2 \int_0^\infty x^2 P_{\text{HDP-FBM}}(x, t) dx = C_p t^{2Hp}. \tag{40}$$

The analytical PDF (38) describes the data of our computer simulations reasonably well, see Fig. 3 obtained for small
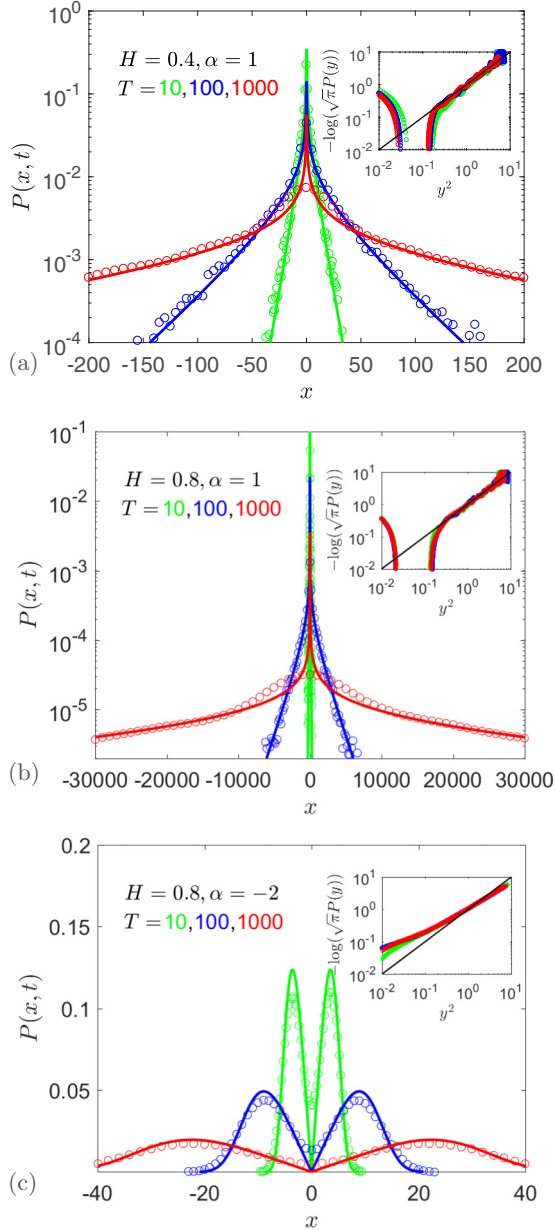
FIG. 3. PDFs of particle displacements for the HDP-FBM model evaluated for the same parameters as used in Fig. 2 (for the corresponding panels). The solid curves in the main plots—with the corresponding colors for varying trajectory lengths T or overall diffusion times $t = T$, as indicated in the legend of each panel—are the analytical predictions for the PDF given by Eq. (38). The insets show the same simulation data in terms of the similarity variable (41) and demonstrate the agreement with the analytical prediction (42) shown as the solid lines (the diagonal in the insets). The initial position of the particles is $x_0 = 10^{-2}$.

initial displacements, $x_0 = 10^{-2}$. Specifically, for the superdiffusive HDPs and slightly subdiffusive FBM—scenario (i) illustrated in Fig. 3(a)—the PDF of the HDP-FBM model is unimodal, with a cusp at $x = 0$. This form is similar to the PDF of pure superdiffusive HDPs, see Eq. (21). The effect of the fractional Gaussian noise at $H = 0.4$ onto the shape of $P_{\text{HDP-FBM}}(x, t)$ as compared to $P_{\text{HDP}}(x, t)$ with the same α

is rather weak (at this H value the FBM dynamics is only slightly subdiffusive).

For superdiffusive HDPs and superdiffusive FBM—scenario (ii) depicted in Fig. 3(b)—the PDF is similarly unimodal, but the smoothening of the PDF cusp for longer trajectories is significantly more pronounced. This effect is particularly visible for the longest trajectories (with $T = t = 10^3$ corresponding to 10^5 simulation steps). We argue, however, that this PDF-smoothening—not captured by the analytical PDF form (38)—has only a marginal effect on the final long-time scaling predictions (35) for the MSD. The latter is dominated by large particle displacements and thus by the tails of $P_{\text{HDP-FBM}}(x, t)$. These tails are indeed correctly described by our analytical form (38), as quantified in the insets of Figs. 3 and 8, compare Eq. (42) below.

For subdiffusive HDPs and superdiffusive FBM—scenario (iii) shown in Fig. 3(c)—the PDF of the HDP-FBM process is bimodal, as the PDF for pure subdiffusive HDPs with $\alpha < 0$ (see Fig. 1(a) in Ref. [77]). For this situation we also detect that the region of slow diffusivity near $x = 0$—depleted of particles for subdiffusive HDPs—becomes populated due to a certain smoothening of $P_{\text{HDP-FBM}}(x, t)$ in the results of simulations. This effect is present also for rather short trajectories, see the data for $T = 10$ in Fig. 3(c).

We confirm the prediction of Eq. (38) for the tails of the PDF obtained by computer simulations. Namely, using the argument of the Gaussian function in (38) as the dimensionless rescaled variable

$$y = \frac{|x|^{1/p}}{(2/p)\sqrt{D_0 t^{2H}}}, \qquad (41)$$

we arrive at the simple Gaussian PDF

$$P_{\text{HDP-FBM}}(y) = \frac{e^{-y^2}}{\sqrt{\pi}}. \qquad (42)$$

To confirm its leading dependence in y—the variable involving the peculiar anomalies of the spacial dynamics [due to $D(x)$] and the temporal dynamics (due to fractional Gaussian noise)—the final PDF for the HDP-FBM model obtained from simulations is plotted in terms of $-\log[\sqrt{\pi}P_{\text{HDP-FBM}}(y)]$ versus y^2 in log-log scale as the insets in Figs. 3 and 8. We observe that in this "natural" renormalized coordinate the long-displacement data from simulations follow the predicted diagonal line in the plots. The universal PDF shape is detected for all trajectory lengths T and all values of the HDP exponent p (both superdiffusive—$p > 1$ and subdiffusive—$0 < p < 1$) as well as all values of the of FBM exponent H (both superdiffusive—$1/2 < H < 1$ and subdiffusive—$0 < H < 1/2$). This supports the universality of the predicted behavior (42), which is one of the central results of the current analysis. Here we also refer to Appendix A for the discussion of similar universal PDF shapes for fractional diffusion equations.

As seen Figs. 3 and 8, for small particle displacements the results of the simulations are not in full agreement with the analytical prediction (42). This fact manifests itself as a "smoothening" of the PDF cusps at $x \to 0$, detected in particular for long trajectories and superdiffusive HDPs choices. In log-log scale of the insets of Fig. 3 this PDF discrepancy at

small x is clearly visible as deviations from (42) at small y^2. This is observed both for superdiffusive [Figs. 3(a) and 3(b)] and subdiffusive [Fig. 3(c)] HDPs. Note that for superdiffusive HDPs the region at small y^2 values, where the deviations of $P_{\text{HDP-FBM}}(y)$ between simulations and theory are observed, does not change with the trajectory length T, see the insets of Figs. 3(a) and 3(b). For longer T, nearly the same region with $P_{\text{HDP-FBM}}(y)$ discrepancies in terms of the y-variable spreads in space for $P_{\text{HDP-FBM}}(x, t)$ in terms of the x variable. For highly subdiffusive HDPs contributing to the HDP-FBM process, the agreement with the prediction (42) is also not perfect (in particular near the origin), see the inset in Fig. 3(c) plotted for $\alpha = -2$. We show in Fig. 8 that for less subdiffusive HDPs (for $\alpha = -1$) the universal slope of $-\log\left[\sqrt{\pi}P_{\text{HDP-FBM}}(y)\right]$ versus y^2 becomes valid in a perceivably larger region of y^2.

A more detailed study of $P_{\text{HDP-FBM}}(x, t)$ near the origin—both for super- and subdiffusive HDPs as well as super- and subdiffusive FBM as parent processes—reveals the relation

$$P_{\text{HDP-FBM}}(x = 0, t) \sim 1/t^{pH}, \quad (43)$$

confirmed by simulations of varying length, see Fig. 9. The behavior of the PDF (43) for small displacements in terms of the similarity variable y is consistent with the functional form

$$P_{\text{HDP-FBM}}(y) \approx \frac{C(p, H)}{\sqrt{\pi}} y^{p-1} e^{-y^2}, \quad (44)$$

as demonstrated in Fig. 10. We emphasize here that this heuristic form of the PDF is not derived, but rather conjectured from the detailed analysis of simulation data for the behavior of the PDF $P_{\text{HDP-FBM}}(y)$ in the region of small y. Specifically, when the data from simulations are divided by the functional form (44), we unveil a plateaulike behavior at small y, universal for all values of the HDP and FBM exponents examined here. The variation of the PDF $P_{\text{HDP-FBM}}(y)$ for different trajectory lengths T is also universal. The normalization constant $C(p, H)$ in Eq. (44) corresponds to the plateau values at $y \to 0$ in Fig. 10. The PDF (44) at small displacements is consistent with the relation (43).

The smoother profiles and finite values of $P_{\text{HDP-FBM}}(x = 0, t)$ at $x \to 0$ obtained in the computer simulations appear instead of the theoretically expected PDF shape (38). Namely, at $p > 1$ we observe no diverging cusp of $P_{\text{HDP-FBM}}(x, t)$ at the origin and at $0 < p < 1$ there is no "inverse cusp" or vanishing $P_{\text{HDP-FBM}}(x, t)$ at the origin. These discrepancies of $P_{\text{HDP-FBM}}(y)$ for the case $p > 1$ can partly stem from a finite (constant) time step in the simulations. Namely, the gradually slowed-down particle dynamics near the origin (with vanishing diffusivities) is not sampled sufficiently frequently to yield the diverging value of $P_{\text{HDP-FBM}}(x = 0, t)$ at $x \to 0$ predicted analytically in Eq. (38). An improved simulation scheme would require certain adjustment of the time step to the value of the local diffusion coefficient. This effect is well documented for diffusion in heterogeneous media and emerges on modeling the spreading dynamics of particles polydisperse in size [138–140]. Given limited computer resources, we could not use a significantly smaller and diffusivity-value-sensitive time step value in these simulations.

The discrepancies of the PDF $P_{\text{HDP-FBM}}(x, t)$ at small x values for the case $p < 1$ can, in turn, also partly originate from

the regularization of $D(x)$ [employed to avoid the divergence at the origin for $\alpha < 0$, Eq. (31)]. We also checked that the disagreement of the PDF close to $x = 0$ stems neither from a particular value for the constant time step δt in the simulation scheme nor from the preset PDF-binning width used to display $P(x, t)$ variations. Different values of δt and of bin widths lead to rather similar results for the PDFs (not shown).

Despite the discrepancies for the PDF $P_{\text{HDP-FBM}}(y)$ at the origin, that we have discussed and quantified, the agreement of the simulations with the theoretical predictions for $P_{\text{HDP-FBM}}(x, t)$ is overall convincing with respect to both position and time dependencies, see the main panels of Fig. 3.

2. Off-center initial conditions

For nonzero initial particle conditions

$$P(x, 0) = \delta(x - x_0), \quad (45)$$

the general analytical expression for the PDF of pure HDPs was derived for an arbitrary stochastic convention $\varkappa$ as (see Eq. (3.57) of Ref. [93])

$$P_{\text{HDP}}(x, t|x_0) = \frac{x^{1/2} x^{(\varkappa-2)\alpha/2} x_0^{1/2} x_0^{-\varkappa\alpha/2}}{(2 - \alpha)D_0 t}$$

$$\times \exp\left[-\frac{x^{2-\alpha} + x_0^{2-\alpha}}{(2 - \alpha)^2 D_0 t}\right] I_{\frac{1-\varkappa\alpha}{\alpha-2}}\left[\frac{2(xx_0)^{\frac{2-\alpha}{2}}}{(2 - \alpha)^2 D_0 t}\right].$$

$$(46)$$

Here $I_j(z)$ denotes the modified Bessel function of the first kind. This expression was obtained for $D(x) = D_0 x^\alpha$ for diffusion on the positive semiaxis $x > 0$ [93]. Analogously to the FBM-based generalization of Eq. (39) and its solution (38), for the general PDF of the HDP-FBM process for initial particle positions sufficiently far away from the origin, we conjecture the form (46) with the simple rescaling

$$t \to t^{2H}. \quad (47)$$

Then, in the Stratonovich representation with $\varkappa = 1/2$ used herein, Eq. (46) leads to (for $x > 0$ only)

$$P_{\text{HDP-FBM}}(x, t|x_0)$$

$$= \frac{x^{3/(2p)-1} x_0^{1/(2p)}}{(2/p)D_0 t^{2H}} \exp\left[-\frac{x^{2/p} + x_0^{2/p}}{(2/p)^2 D_0 t^{2H}}\right] I_{-1/2}\left[\frac{2(xx_0)^{1/p}}{(2/p)^2 D_0 t^{2H}}\right].$$

$$(48)$$

For small arguments of $I_{-1/2}(z_0)$ in Eq. (48), namely at

$$z_0 = \frac{2(xx_0)^{1/p}}{(2/p)^2 D_0 t^{2H}} \ll 1, \quad (49)$$

using $I_{-1/2}(z_0) \approx \sqrt{2/(\pi z_0)}$ we arrive at the PDF (38). In the opposite limit $z_0 \gg 1$ we use the expansion $I_{-1/2}(z_0) \approx e^{z_0}/\sqrt{2\pi z_0}$ and (for $x_0 > 0$) arrive at the "shifted" stretched or compressed Gaussian

$$P_{\text{HDP-FBM}}(x, t|x_0) \approx \frac{x^{1/p-1} \exp\left\{-\left[\frac{x^{1/p}-x_0^{1/p}}{(2/p)\sqrt{D_0 t^{2H}}}\right]^2\right\}}{\sqrt{4\pi D_0 t^{2H}}}. \quad (50)$$

In Fig. 11 we quantify the region of the model parameters x and T as well as of the HDP and FBM exponents for which
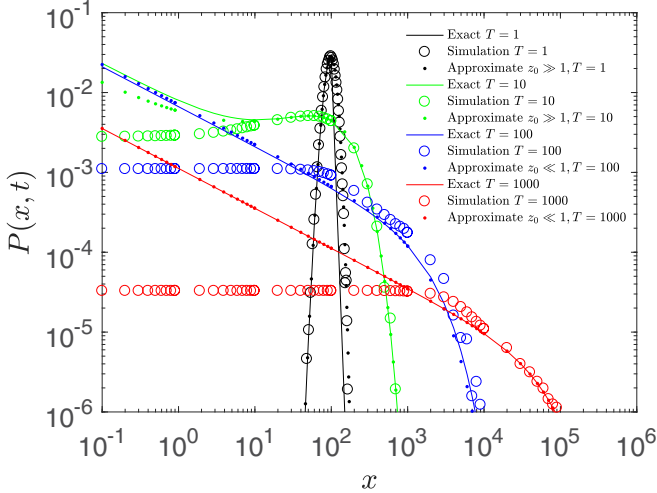
FIG. 4. PDF of the HDP-FBM process $P_{\text{HDP-FBM}}(x, t|x_0)$ (shown on the positive half-axis only) for $\alpha = 1$, $H = 0.8$, and (strongly) off-centered initial particle position, $x_0 = 10^2$. Results of simulations are the empty colored circles, the analytical PDF prediction (48) are the solid curves, the large-argument approximation (50) are the dots in the large-z_0 regime, and the approximate small-argument analytical results (38) are the dots in the large-z_0 region (see the legend). The results of these approximations are shown in the region of x and T and for exponents H and α when the conditions $z_0 \gg 1$ and $z_0 \ll 1$ are satisfied, correspondingly (see Fig. 11). The color scheme is the same as in Fig. 3 (see the legend).

the conditions $z_0 \gg 1$ and $z_0 \ll 1$ are valid (for a given initial position x_0).

In Fig. 4 we demonstrate that the results of computer simulations for the PDF $P_{\text{HDP-FBM}}(x, t|x_0)$ at large off-centered initial particle positions. The HDP and FBM exponents chosen here as $\alpha = 1$ and $H = 0.8$ [the same as in Figs. 2(b) and 3(b)]. At very long times, we find that the influence of nonzero x_0 progressively diminishes and the PDF becomes insensitive to the initial position. Naturally, this happens on shorter time-scales for superdiffusive realizations of the HDP-FBM process, as compared to subdiffusive ones (results not shown). For the initial stage of the diffusion process, the particles are almost exclusively in the half-space $x > 0$ near $x = x_0$ and the PDF expression (48) is used, see the data for $T = 10^0$ and 10^1 in Fig. 4. The data are well described by Eqs. (48) and (50) in the entire region of particle positions. In the long-time limit, the effects of nonzero x_0 are almost lost and the PDF becomes nearly symmetric with respect to $x = 0$ (results not shown). To describe the simulations data, the half-space PDF (48) should then be divided by 2 for proper normalization, see the data obtained for $T = 10^2$ and 10^3 in Fig. 4.

We quantify the tails of the PDF $P_{\text{HDP-FBM}}(x, t|x_0)$ for nonzero x_0 in terms of the shifted variable $(y - y_0)^2$ via plotting the PDF data from simulations in Fig. 12. Here y_0 is computed via (41) for x_0. Using the large-displacement PDF (50) we then arrive at

$$P_{\text{HDP-FBM}}(y|y_0) = \frac{e^{-(y-y_0)^2}}{\sqrt{\pi}}, \qquad (51)$$

with this leading functional dependence being scaled out in the presentation of Fig. 12 (for the case of subdiffusive parent HDPs). We find that for all choices of the HDP and FBM exponents considered in Fig. 3 the tails of the off-centered PDFs $P_{\text{HDP-FBM}}(y|y_0)$ are consistent with the simple form (51).

We argue, however, that the PDF (48) only describes well the long tails of the $P_{\text{HDP-FBM}}(x, t|x_0)$ data, while in the region of small particle displacements the analytical predictions (48) and (38) fail to match the simulation data. In fact, expression (50) cannot be applied in this region as well, because the condition $z_0 \gg 1$ is not always satisfied. This discrepancy between simulations and theory in the region of small x manifests itself in the same PDF "smoothening", as observed in Figs. 3 and 8.

We checked the validity of the scaling relation (43) for substantially off-center initial particle positions for sufficiently long trajectories (after the overall symmetric PDFs have been established). We present the PDF results for sub- and superdiffusive parent HDPs in Figs. 13 and 15, correspondingly. For short trajectories, naturally, the scaling (43) is not valid because no symmetry of the PDF with respect to $x = 0$ has been achieved yet. For short simulation times, the starting positions are clearly visible from the PDF, while at long times the PDF shape is nearly symmetric with respect to $x = 0$.

The validity of Eq. (43) for off-center initial positions at long simulation times is demonstrated by simulations for both sub- and superdiffusive HDPs in the HDP-FBM model in Figs. 14 and 16, respectively. Thus, the PDF deviations we detected near $x = 0$ in Figs. 3 and 8 are no artifacts of some close-to-zero x_0 positions chosen in the simulations (e.g., $x_0 = 10^{-2}$). We also observe that as the initial particle position $|x_0|$ is shifted away from the origin, naturally, the simulation times (or the trajectory lengths T) required to reach nearly symmetric PDF shapes also increase. As a result, the universal scaling relation (43) starts to be followed at longer T (with nearly symmetric PDFs), as demonstrated in Fig. 16. Nevertheless, at this point we cannot unequivocally identify distinct mechanisms for the discrepancies between simulations and theoretical predictions for the PDF $P_{\text{HDP-FBM}}(x, t)$ at small x.

V. DISCUSSION AND CONCLUSIONS

We presented the results of computer simulations of a combined HDP-FBM stochastic process. We analyzed the statistical properties of this anomalous-diffusion process based on the MSD and TAMSD as well as the displacement PDF. We compared and contrasted its characteristics to those of the parent processes, FBM and HDPs. Specifically, we confirmed that in a large range of HDP and FBM exponents α and H, as demonstrated in Fig. 1, the scaling relations for the MSD and mean TAMSD of the HDP-FBM process are similar to those for HDPs with the intuitive redefinition of the exponents,

$$\left\langle x_{\text{HDP}}^2(t) \right\rangle \simeq t^{\frac{2}{2-\alpha}} \rightarrow \left\langle x_{\text{HDP-FBM}}^2(t) \right\rangle \simeq t^{\frac{2}{2-\alpha} \times 2H} \qquad (52)$$

and

$$\left\langle \overline{\delta_{\text{HDP}}^2(\Delta)} \right\rangle \simeq \Delta^1 \rightarrow \left\langle \overline{\delta_{\text{HDP-FBM}}^2(\Delta)} \right\rangle \simeq \Delta^{2H}. \qquad (53)$$

This indicates that the effects of the position-dependent diffusivity and of fractional Gaussian noise are independent from one another in their impact onto the particle dynamics. This conclusion is similar to that obtained for the HDP-SBM model considered in Ref. [82].

For stochastic processes with multiplicative noise, here due to position-dependent diffusivity $D(x)$, several questions have been addressed in the literature: namely, those of consistent formulations of the general statistical mechanics, differences in the over- and underdamped limits, generalization of the fluctuation-dissipation theorem (the Stokes-Einstein relation), equilibration of the particles and the modified Boltzmann distribution as its measure, and the emergence of the "spurious drift" [110,119,120,141–143], as well as self-consistent links between the space-local diffusivity and damping [83,95,144–152]. For a thermally equilibrated particle the thermodynamic consistency can only be satisfied in the Hänggi-Klimontovich convention [110]. The definition of an effective temperature—a measure of the average kinetic energy, $m\langle v^2 \rangle/2 = k_B T/2$, of the diffusing particle based on the Maxwell-Boltzmann statistics, where k_B is the Boltzmann constant—was also discussed in some of these studies (for the underdamped Langevin equation for a particle of mass m). These general questions for the current HDP-FBM system deserve special consideration. We note, however, that in the realm of living biological cells with their plethora of energy-consuming, active molecular processes the assumption of equilibrium cannot be made *a priori* and thus the discussion of the general effects in this work is physically legitimate.

The spectrum of physical systems for the HDP-FBM model includes, i.e., the above listed HDP-relevant systems driven now by fractional (instead of white Gaussian) noise. The occurrence of the correlated noise in these systems is expected, e.g., in biological cells and artificially crowded liquids in which "passive-antipersistence" of the noise is due to crowding, while "active-persistent" noise arises for active processes such as motor-driven motion. The deterministic structural disorder is given by the cell morphology or the designed pore properties of a given environment, such as hydrogels. Evidently, as a first step, the applicability of the overdamped approximation (30) to the dynamics at short-to-intermediate times, the specific choice of the power-law position-dependence (16) of the diffusion coefficient $D(x)$ and the power-law time decay of the increment correlations (5) need to be validated for a specific system. For instance, the increment correlations of the fractional Gaussian noise may have to be cut-off in system-specific ways [153] or some modifications of the power-law forms of $D(x)$ may be needed.

We also note that the current results can also be applied, e.g., to the inverse problem of inferring the spatial scaling exponent of the $D(x)$ dependence and the Hurst exponent of FBM from analyzing the decay of the tails of the PDF $P_{\text{HDP-FBM}}(x,t)$ that are sensitive to the underlying space-time dynamics, as evidenced by Eq. (41).

ACKNOWLEDGMENTS

APPENDIX A: PDFS

We note the remarkable similarity between the bimodal double-hump PDF form (38) featured by subdiffusive HDPs and the large-displacement tails of the PDF satisfying the fractional wave equations [154–156] (with $0 < \beta \leqslant 1$)

$$\frac{\partial^2}{\partial t^2} P_{\text{FWE}}(x,t)$$
$$= K_{2-\beta} \frac{\partial}{\partial t} \left[\frac{1}{\Gamma(\beta)} \int_0^t \frac{dt'}{(t-t')^{1-\beta}} \frac{\partial^2}{\partial x^2} P_{\text{FWE}}(x,t') \right]. \quad (A1)$$

For this case, however, the PDF with the two off-center humps is realized for superdiffusive (rather than subdiffusive) MSD growth,

$$\langle x_{\text{FWE}}^2(t) \rangle = \frac{2K_{2-\beta}}{\Gamma(3-\beta)} t^{2-\beta}. \quad (A2)$$

We refer the reader to Fig. 1 and Eq. (6) in Ref. [156] as well as to Fig. 4 and Eq. (38) in Ref. [155] describing the compressed-Gaussian tails of the respective PDFs. Interestingly, in terms of a new universal rescaled variable,

$$y_\beta^2 = \frac{\beta}{2} \left(\frac{2-\beta}{2} \right)^{\frac{2-\beta}{\beta}} \left(\frac{|x|}{\sqrt{K_{2-\beta} t^{2-\beta}}} \right)^{2/\beta}, \quad (A3)$$

these expressions for the PDF tails yield a simple Gaussian (42),

$$P_{\text{FWE}}(y_\beta) \approx e^{-y_\beta^2} / \sqrt{(2-\beta)\pi}. \quad (A4)$$

For $\beta \to 1$ we get $y_\beta^2 \to x^2/(4K_1 t)$ and Eq. (A4) reduces to the canonical Gaussian (42).

For the subdiffusive fractional diffusion equation $(0 < \bar{\beta} < 1)$ of the form

$$\frac{\partial}{\partial t} P_{\text{FDE}}(x,t) = \frac{K_{\bar{\beta}}}{\Gamma(\bar{\beta})} \frac{\partial}{\partial t} \left[\int_0^t \frac{dt'}{(t-t')^{1-\bar{\beta}}} \frac{\partial^2}{\partial x^2} P_{\text{FDE}}(x,t) \right], \quad (A5)$$

the long tails of the PDF obeys the stretched-Gaussian form (e.g., see Eq. (45) in Ref. [4]). The PDF (A5) with the characteristic cusp at the origin also leads to the Gaussian (A4) in terms of the variable y_β and the redefined exponent

$$\bar{\beta} \to (2 - \beta). \quad (A6)$$

APPENDIX B: AUXILIARY FIGURES

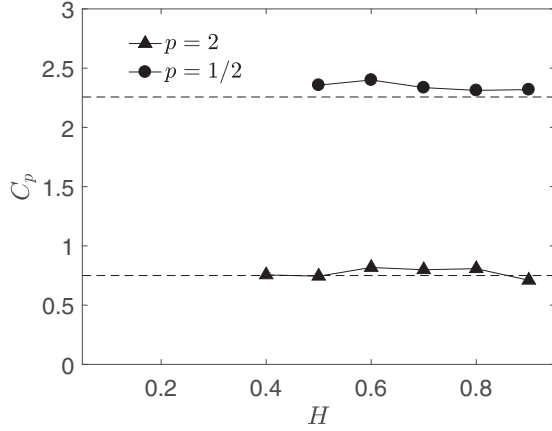Below, we present some additional figures supporting our claims in the main text.

FIG. 5. Variation of the prefactor C_p versus H for the HDP-FBM process as computed from fitting the MSD magnitude in simulations (symbols) and predicted from Eq. (19) theoretically (black dashed lines). The values of the HDP exponent p are provided in the legend. Other parameters are the same as in Fig. 2.
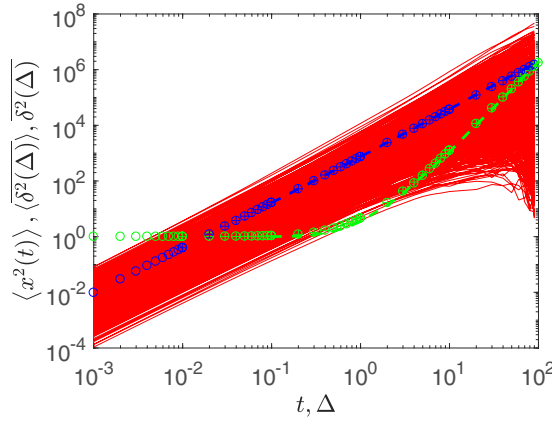

FIG. 8. PDF of particle displacements for the HDP-FBM model (the parameters and trajectory lengths are given in the legend). The inset presents the same data as well as the analytical form (42) in terms of y^2. Other parameters are the same as in Fig. 3 and $x_0 = 10^{-2}$.

FIG. 6. Insensitivity of the MSD and TAMSD variations to the time-step magnitude used in simulations. Parameters: $H = 0.8$, $\alpha = 1$ [like in Fig. 2(b)], $x_0 = 1$, $\delta t = 10^{-1}$ (dashed curves), 10^{-2} (crosses), and 10^{-3} (circles).
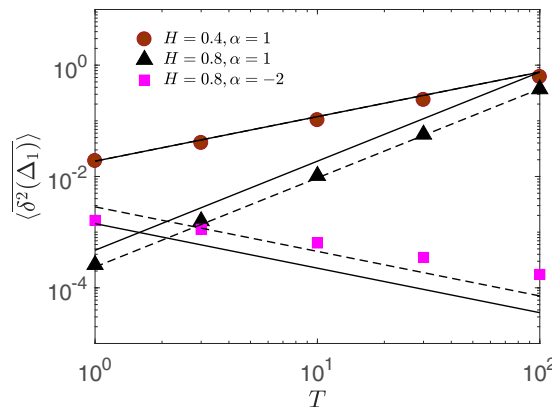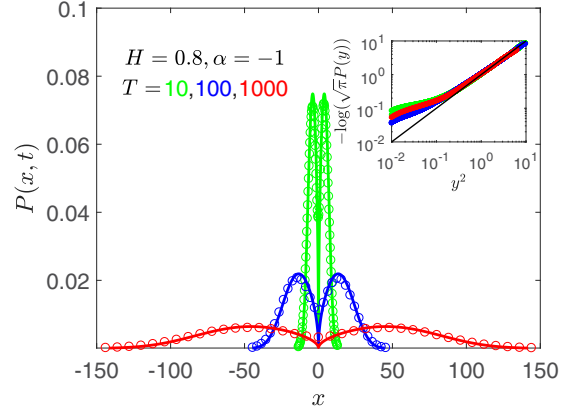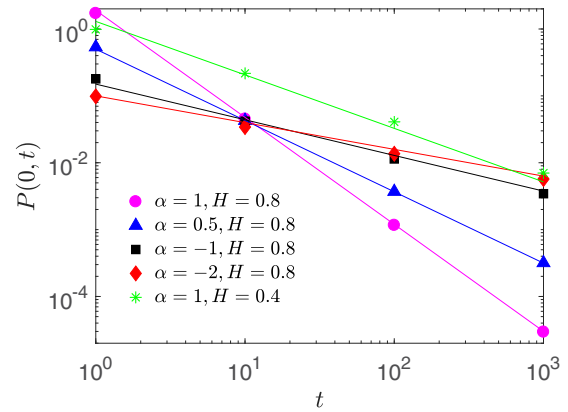

FIG. 9. Magnitude of $P_{\mathrm{HDP\text{-}FBM}}(x = 0, t)$ evaluated for different values of the exponents of the parent HDPs and FBM processes and plotted for varying simulation time t. Scaling relation (43) is shown as the solid asymptotes.
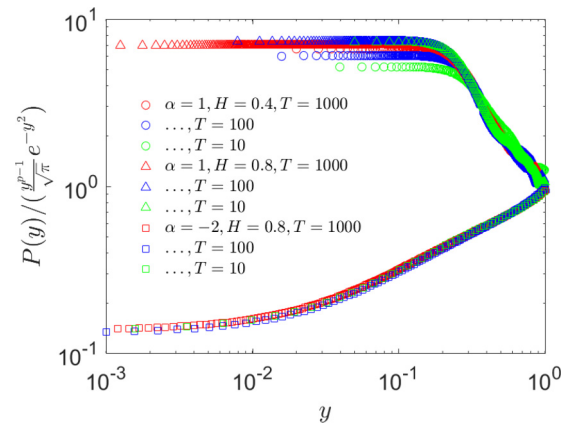

FIG. 7. Variation of initial TAMSD values, $\overline{\delta^2_{\mathrm{HDP\text{-}FBM}}(\Delta_1)}$, computed for the parameters of Figs. 2(a), 2(b), and 3(c) and plotted here for varying trajectory length, T. The solid black lines are the exact theoretical predictions (24), while the dashed lines are amplitude-shifted scaling predictions (shown for clarity).

FIG. 10. Simulation data for $P_{\mathrm{HDP\text{-}FBM}}(y)$ renormalized by the PDF form (44), yielding $C(p, H)$ as the plateau value at small y. The HDP and FBM exponents are the same as in Fig. 3 (see the legend); the same color scheme is also used for the data at different diffusion times t (or total trajectory lengths, T). The plateau region at small y is also observed for other model parameters of Fig. 9 (results not shown).
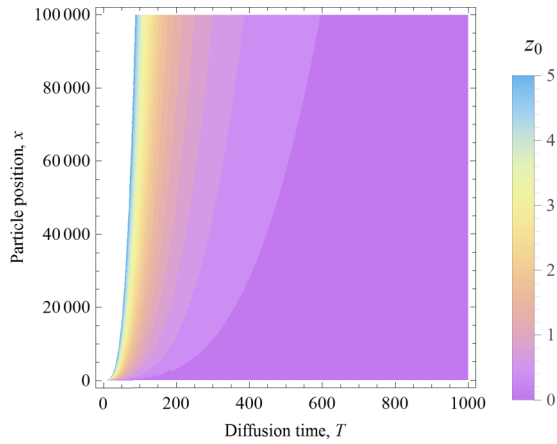
FIG. 11. Regions of small and large arguments z_0 shown for varying values of x and T (plotted for H, α, and x_0 values of Fig. 4).

FIG. 14. Scaling of the PDF value at $x = 0$ versus the diffusion time t for different initial positions x_0, as indicated in the legend. The dashed line denotes the scaling relation (43). Other parameters are the same as in Fig. 13. The missing points for shorter trajectory lengths correspond to the extremely low PDF values at $x = 0$, outside of the relevant range shown in the plot.
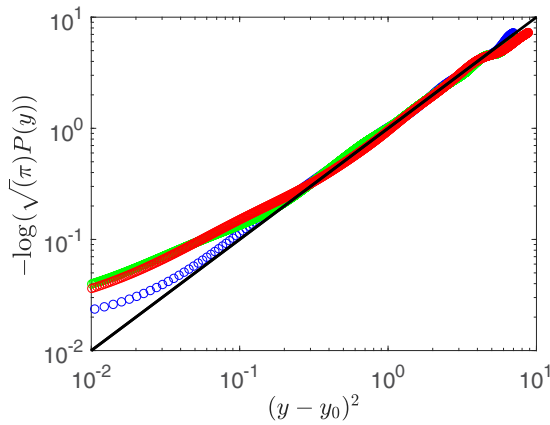

FIG. 12. Tails of $P_{\text{HDP-FBM}}(y|y_0)$ (the simulated data shown for the positive half-space) after rescaling the leading functional dependence (51) plotted versus the shifted space-time variable $(y - y_0)^2$. The model parameters and the color scheme are the same as in Fig. 8, except $x_0 = 10^2$.
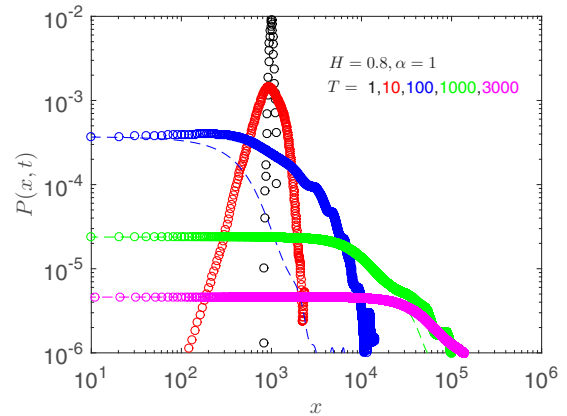
FIG. 15. PDFs for the starting position $x_0 = 10^3$ in the HDP-FBM model, for superdiffusive FBM with the exponent $H = 0.8$ and for superdiffusive HDPs with the exponent $\alpha = 1$ [as in Fig. 2(b)]. The dashed curves indicate the respective PDF variations at $x < 0$ mirrored into the region $x > 0$, shown in the corresponding color for different trajectory lengths T (see the legend).
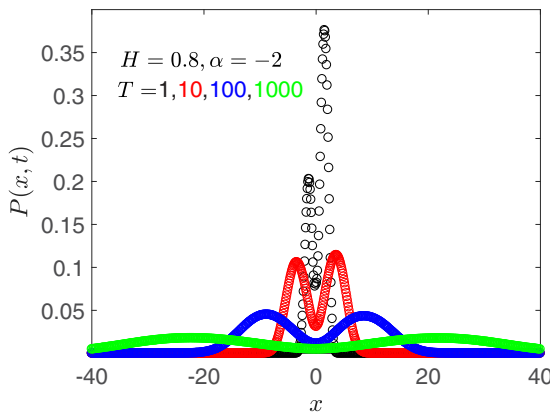

FIG. 13. PDF $P_{\text{HDP-FBM}}(x, t|x_0)$ for the off-center initial position, $x_0 = 1$, and subdiffusive parent HDPs. The trajectory lengths $T = t$ are indicated in the legend by the respective color. Other parameters: $H = 0.8$ and $\alpha = -2$ [as in Fig. 2(c)].
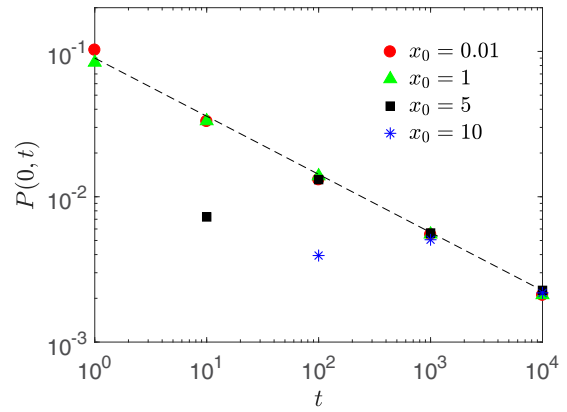

FIG. 16. The same as in Fig. 14, but for the parameters of Fig. 15 (namely $H = 0.8$ and $\alpha = 1$). The dashed line is the asymptote (43).

[1] J. W. Haus and K. W. Kehr, Diffusion in regular and disordered lattices, Phys. Rep. **150**, 263 (1987).

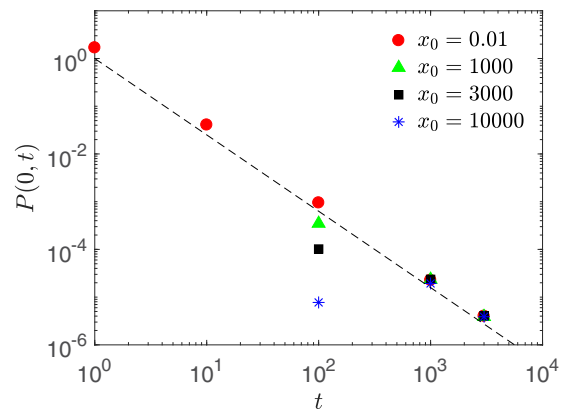[2] J.-P. Bouchaud and A. Georges, Anomalous diffusion in disordered media: Statistical mechanisms, models and physical applications, Phys. Rep. **195**, 127 (1990).

[3] S. Havlin and D. Ben-Avraham, Diffusion in disordered media, Adv. Phys. **51**, 187 (2002).

[4] R. Metzler and J. Klafter, The random walk's guide to anomalous diffusion: A fractional dynamics approach, Phys. Rep. **339**, 1 (2000).

[5] R. Metzler and J. Klafter, The restaurant at the end of the random walk: Recent developments in the description of anomalous transport by fractional dynamics, J. Phys. A **37**, R161 (2004).

[6] S. Burov, J.-H. Jeon, R. Metzler, and E. Barkai, Single particle tracking in systems showing anomalous diffusion: The role of weak ergodicity breaking, Phys. Chem. Chem. Phys. **13**, 1800 (2011).

[7] E. Barkai, Y. Garini, and R. Metzler, Strange kinetics of single molecules in living cells, Phys. Today **65**(8), 29 (2012).

[8] V. Zaburdaev, S. Denisov, and J. Klafter, Lévy walks, Rev. Mod. Phys. **87**, 483 (2015).

[9] I. M. Sokolov, Models of anomalous diffusion in crowded environments, Soft Matter **8**, 9043 (2012).

[10] F. Höfling and T. Franosch, Anomalous transport in the crowded world of biological cells, Rep. Prog. Phys. **76**, 046602 (2013).

[11] R. Metzler, J.-H. Jeon, A. G. Cherstvy, and E. Barkai, Anomalous diffusion models and their properties: Non-stationarity, non-ergodicity, and ageing at the centenary of single particle tracking, Phys. Chem. Chem. Phys. **16**, 24128 (2014).

[12] Y. Meroz and I. M. Sokolov, A toolbox for determining subdiffusive mechanisms, Phys. Rep. **573**, 1 (2015).

[13] R. Metzler, J.-H. Jeon, and A. G. Cherstvy, Non-Brownian diffusion in lipid membranes: Experiments and simulations, Biochem. Biophys. Acta BBA-Biomembr. **1858**, 2451 (2016).

[14] D. Krapf and R. Metzler, Strange interfacial molecular dynamics, Phys. Today **72**(9), 48 (2019).

[15] M. Weiss, M. Elsner, F. Kartberg, and T. Nilsson, Anomalous subdiffusion is a measure for cytoplasmic crowding in living cells, Biophys J. **87**, 3518 (2004).

[16] A. Caspi, R. Granek, and M. Elbaum, Enhanced Diffusion in Active Intracellular Transport, Phys. Rev. Lett. **85**, 5655 (2000).

[17] G. Seisenberger, M. U. Ried, T. Endreß, H. Büning, M. Hallek, and C. Bräuchle, Real-time single-molecule imaging of the infection pathway of an adeno-associated virus, Science **294**, 1929 (2001).

[18] I. Golding and E. C. Cox, Physical Nature of Bacterial Cytoplasm, Phys. Rev. Lett. **96**, 098102 (2006).

[19] J.-H. Jeon, V. Tejedor, S. Burov, E. Barkai, C. Selhuber-Unkel, K. Berg-Sørensen, L. Oddershede, and R. Metzler, *In Vivo* Anomalous Diffusion and Weak Ergodicity Breaking of Lipid Granules, Phys. Rev. Lett. **106**, 048103 (2011).

[20] S. M. A. Tabei, S. Burov, H. Y. Kim, A. Kuznetsov, T. Huynh, J. Jureller, L. H. Philipson, A. R. Dinner, and N. F. Scherer, Intracellular transport of insulin granules is a subordinate, Proc. Natl. Acad. Sci. USA **110**, 4911 (2013).

[21] D. S. Banks and C. Fradin, Anomalous diffusion of proteins due to molecular crowding, Biophys. J. **89**, 2960 (2005).

[22] J. Szymanski and M. Weiss, Elucidating the Origin of Anomalous Diffusion in Crowded Fluids, Phys. Rev. Lett. **103**, 038102 (2009).

[23] J.-H. Jeon, N. Leijnse, L. B. Oddershede, and R. Metzler, Anomalous diffusion and power-law relaxation of the time averaged mean squared displacement in worm-like micellar solutions, New J. Phys. **15**, 045011 (2013).

[24] M. Weiss, H. Hashimoto, and T. Nilsson, Anomalous protein diffusion in living cells as seen by fluorescence correlation spectroscopy, Biophys. J. **84**, 4043 (2003).

[25] A. V. Weigel, B. Simon, M. M. Tamkun, and D. Krapf, Ergodic and nonergodic processes coexist in the plasma membrane as observed by single-molecule tracking, Proc. Natl. Acad. Sci. USA **108**, 6438 (2011).

[26] C. Manzo, J. A. Torreno-Pina, P. Massignan, G. J. Lapeyre Jr, M. Lewenstein, and M. F. Garcia Parajo, Weak Ergodicity Breaking of Receptor Motion in Living Cells Stemming from Random Diffusivity, Phys. Rev. X **5**, 011021 (2015).

[27] W. He, H. Song, Y. Su, L. Geng, B. J. Ackerson, H. B. Peng, and P. Tong, Dynamic heterogeneity and non-Gaussian statistics for acetylcholine receptors on live cell membrane, Nat. Commun. **7**, 11701 (2016).

[28] G. R. Kneller, K. Baczynski, and M. Pasenkiewicz-Gierula, Communication: Consistent picture of lateral subdiffusion in lipid bilayers: Molecular dynamics simulation and exact results, J. Chem. Phys. **135**, 141105 (2011).

[29] J.-H. Jeon, H. Martinez-Seara Monne, M. Javanainen, and R. Metzler, Anomalous Diffusion of Phospholipids and Cholesterols in a Lipid Bilayer and its Origins, Phys. Rev. Lett. **109**, 188103 (2012).

[30] J.-H. Jeon, M. Javanainen, H. Martinez-Seara, R. Metzler, and I. Vattulainen, Protein Crowding in Lipid Bilayers Gives Rise to Non-Gaussian Anomalous Lateral Diffusion of Phospholipids and Proteins, Phys. Rev. X **6**, 021006 (2016).

[31] X. Hu, L. Hong, M. D. Smith, T. Neusius, X. Cheng, and J. C. Smith, The dynamics of single protein molecules is non-equilibrium and self-similar over thirteen decades in time, Nat. Phys. **12**, 171 (2016).

[32] D. Robert, T. H. Nguyen, F. Gallet, and C. Wilhelm, *In vivo* determination of fluctuating forces during endosome trafficking using a combination of active and passive microrheology, PLoS ONE **5**, e10046 (2010).

[33] J. F. Reverey, J.-H. Jeon, H. Bao, M. Leippe, R. Metzler, and C. Selhuber-Unkel, Superdiffusion dominates intracellular particle motion in the supercrowded cytoplasm of pathogenic Acanthamoeba castellanii, Sci. Rep. **5**, 11690 (2015).

[34] M. S. Song, H. C. Moon, J.-H. Jeon, and H. Y. Park, Neuronal messenger ribonucleoprotein transport follows an aging Lévy walk, Nat. Commun. **9**, 344 (2018).

[35] K. J. Chen, B. Wang, and S. Granick, Memoryless self-reinforcing directionality in endosomal active transport within living cells, Nat. Mater. **14**, 589 (2015).

[36] E. W. Montroll and G. H. Weiss, Random walks on lattices. II, J. Math. Phys. **6**, 167 (1965).

[37] E. W. Montroll, Random walks on lattices. III. Calculation of first-passage times with application to exciton trapping on photosynthetic units, J. Math. Phys. **10**, 753 (1969).

[38] H. Scher and E. W. Montroll, Anomalous transit-time dispersion in amorphous solids, Phys. Rev. B **12**, 2455 (1975).

[39] J.-H. Jeon, A. V. Chechkin and R. Metzler, Scaled Brownian motion: A paradoxical process with a time dependent diffusivity for the description of anomalous diffusion, Phys. Chem. Chem. Phys. **16**, 15811 (2014).

[40] H. Safdari, A. G. Cherstvy, A. V. Chechkin, A. Bodrova, and R. Metzler, Aging underdamped scaled Brownian motion: Ensemble- and time-averaged particle displacements, nonergodicity, and the failure of the overdamping approximation, Phys. Rev. E **95**, 012120 (2017).

[41] A. N. Kolmogorov, Wienersche Spiralen und einige andere interessante Kurven im Hilbertschen Raum, C. R. (Doklady) Acad. Sci. URSS (N.S.) **26**, 115 (1940).

[42] A. M. Yaglom, Correlation theory of processes with random stationary nth increments, AMS Transl. **2**, 87 (1958).

[43] B. B. Mandelbrot and J. W. van Ness, Fractional Brownian motions, fractional noises and applications, SIAM Rev. **10**, 422 (1968).

[44] A. M. Yaglom, *Correlation Theory of Stationary and Related Random Functions* (Springer, Heidelberg, 1987).

[45] W. Deng and E. Barkai, Ergodic properties of fractional Brownian-Langevin motion, Phys. Rev. E **79**, 011112 (2009).

[46] I. Goychuk, Viscoelastic subdiffusion: Generalized Langevin equation approach, Adv. Chem. Phys. **150**, 187 (2012).

[47] S. C. Weber, A. J. Spakowitz, and J. A. Theriot, Bacterial Chromosomal Loci Move Subdiffusively Through a Viscoelastic Cytoplasm, Phys. Rev. Lett. **104**, 238102 (2010).

[48] K. Burnecki, E. Kepten, J. Janczura, I. Bronshtein, Y. Garini, and A. Weron, Universal algorithm for identification of fractional Brownian motion. A case of telomere subdiffusion, Biophys. J. **103**, 1839 (2012).

[49] E. Lutz, Fractional Langevin equation, Phys. Rev. E **64**, 051106 (2001).

[50] T. Guggenberger, G. Pagnini, T. Vojta, and R. Metzler, Fractional Brownian motion in a finite interval: Correlations effect depletion or accretion zones of particles near boundaries, New J. Phys. **21**, 022002 (2019).

[51] T. Vojta, S. Skinner, and R. Metzler, Probability density of the fractional Langevin equation with reflecting walls, Phys. Rev. E **100**, 042142 (2019).

[52] J.-P. Bouchaud, Weak ergodicity breaking and aging in disordered systems, J. Phys. (Paris) I **2**, 1705 (1992).

[53] J. L. Lebowitz and O. Penrose, Modern ergodic theory, Phys. Today **26**, 23 (1973).

[54] A. Andereanov and D. S. Grebenkov, Time-averaged MSD of Brownian motion, J. Stat. Mech. (2012) P07001.

[55] A. G. Cherstvy, S. Thapa, Y. Mardoukhi, A. V. Chechkin, and R. Metzler, Time averages and their statistical variation for the Ornstein-Uhlenbeck process: Role of initial particle conditions and relaxation to stationarity, Phys. Rev. E **98**, 022134 (2018).

[56] M. Schwarzl, A. Godec, and R. Metzler, Quantifying nonergodicity of anomalous diffusion with higher order moments, Sci. Rep. **7**, 3878 (2017).

[57] J.-H. Jeon and R. Metzler, Fractional Brownian motion and motion governed by the fractional Langevin equation in confined geometries, Phys. Rev. E **81**, 021103 (2010).

[58] J.-H. Jeon and R. Metzler, Inequivalence of time and ensemble averages in ergodic systems: exponential versus power-law relaxation in confinement, Phys. Rev. E **85**, 021147 (2012).

[59] M. V. Chubynsky and G. W. Slater, Diffusing Diffusivity: A Model for Anomalous, Yet Brownian, Diffusion, Phys. Rev. Lett. **113**, 098302 (2014).

[60] T. Uneyama, T. Miyaguchi, and T. Akimoto, Fluctuation analysis of time-averaged mean-square displacement for the Langevin equation with time-dependent and fluctuating diffusivity, Phys. Rev. E **92**, 032140 (2015).

[61] A. V. Chechkin, F. Seno, R. Metzler, and I. M. Sokolov, Brownian yet Non-Gaussian Diffusion: From Superstatistics to Subordination of Diffusing Diffusivities, Phys. Rev. X **7**, 021002 (2017).

[62] W. Wang, A. G. Cherstvy, A. V. Chechkin, S. Thapa, F. Seno, X. Liu, and R. Metzler, Fractional Brownian motion with random diffusivity: emerging residual nonergodicity below the correlation time, J. Phys. A (2020), doi:10.1088/1751-8121/aba467.

[63] D. Molina-Garcia, T. M. Pham, P. Paradisi, C. Manzo, and G. Pagnini, Fractional kinetics emerging from ergodicity breaking in random media, Phys. Rev. E **94**, 052147 (2016).

[64] M. Magdziarz, A. Weron, K. Burnecki, and J. Klafter, Fractional Brownian Motion Versus the Continuous-Time Random Walk: A Simple Test for Subdiffusive Dynamics, Phys. Rev. Lett. **103**, 180602 (2009).

[65] E. Kepten, I. Bronshtein, and Y. Garini, Ergodicity convergence test suggests telomere motion obeys fractional dynamics, Phys. Rev. E **83**, 041919 (2011).

[66] M. Weiss, Resampling single-particle tracking data eliminates localization errors and reveals proper diffusion anomalies, Phys. Rev. E **100**, 042125 (2019).

[67] D. Ernst, J. Kohler, and M. Weiss, Probing the type of anomalous diffusion with single-particle tracking, Phys. Chem. Chem. Phys. **16**, 7686 (2014).

[68] M. P. Backlund, R. Joyner, and W. E. Moerner, Chromosomal locus tracking with proper accounting of static and dynamic errors, Phys. Rev. E **91**, 062716 (2015).

[69] S. C. Weber, M. A. Thompson, W. E. Moerner, A. J. Spakowitz, and J. A. Theriot, Analytical tools to distinguish the effects of localization error, confinement, and medium elasticity on the velocity autocorrelation function, Biophys. J. **102**, 2443 (2012).

[70] D. Krapf, Mechanisms underlying anomalous diffusion in the plasma membrane, Curr. Topics Membr. **75**, 167 (2015).

[71] O. Pulkkinen and R. Metzler, Distance Matters: The Impact of Gene Proximity in Bacterial Gene Regulation, Phys. Rev. Lett. **110**, 198101 (2013).

[72] L. Mirny, M. Slutsky, Z. Wunderlich, A. Tafvizi, J. Leith, A. Kosmrlj, How a protein searches for its site on DNA: The mechanism of facilitated diffusion, J. Phys. A **42**, 434013 (2009).

[73] Y. Lanoiselee, N. Moutal, and D. S. Grebenkov, Diffusion-limited reactions in dynamic heterogeneous media, Nat. Commun. **9**, 4398 (2018).

[74] A. Godec and R. Metzler, Universal Proximity Effect in Target Search Kinetics in the Few-Encounter Limit, Phys. Rev. X **6**, 041037 (2016)

[75] M. Hellmann, D. W. Heermann, and M. Weiss, Enhancing phosphorylation cascades by anomalous diffusion, Europhys. Lett. **97**, 58004 (2012).

[76] L. Liu, A. G. Cherstvy, and R. Metzler, Facilitated diffusion of transcription factor proteins with anomalous bulk diffusion, J. Phys. Chem. B **121**, 1284 (2017).

[77] A. G. Cherstvy, A. V. Chechkin, and R. Metzler, Anomalous diffusion and ergodicity breaking in heterogeneous diffusion processes, New J. Phys. **15**, 083039 (2013).

[78] A. G. Cherstvy and R. Metzler, Population splitting, trapping, and non-ergodicity in heterogeneous diffusion processes, Phys. Chem. Chem. Phys. **15**, 20220 (2013).

[79] A. G. Cherstvy, A. V. Chechkin, and R. Metzler, Particle invasion, survival, and non-ergodicity in 2D diffusion processes with space-dependent diffusivity, Soft Matter **10**, 1591 (2014).

[80] A. G. Cherstvy, A. V. Chechkin, and R. Metzler, Ageing and confinement in non-ergodic heterogeneous diffusion processes, J. Phys. A **47**, 485002 (2014).

[81] A. G. Cherstvy and R. Metzler, Nonergodicity, fluctuations, and criticality in heterogeneous diffusion processes, Phys. Rev. E **90**, 012134 (2014).

[82] A. G. Cherstvy and R. Metzler, Ergodicity breaking, ageing, and confinement in generalized diffusion processes with position and time dependent diffusivity, J. Stat. Mech. (2015) P05010.

[83] A. W. C. Lau and T. C. Lubensky, State-dependent diffusion: Thermodynamic consistency and its path integral formulation, Phys. Rev. E **76**, 011123 (2007).

[84] L. F. Richardson, Atmospheric diffusion shown on a distance-neighbour graph, Proc. R. Soc. Lond. A **110**, 709 (1926).

[85] H. G. E. Hentschel and I. Procaccia, Relative diffusion in turbulent media: The fractal dimension of clouds, Phys. Rev. A **29**, 1461 (1984).

[86] B. O'Shaugnessy and I. Procaccia, Analytical Solutions for Diffusion on Fractal Objects, Phys. Rev. Lett. **54**, 455 (1985).

[87] B. O'Shaugnessy and I. Procaccia, Diffusion on fractals, Phys. Rev. A **32**, 3073 (1985).

[88] J. Klafter, A. Blumen, and M. F. Shlesinger, Stochastic pathway to anomalous diffusion, Phys. Rev. A **35**, 3081 (1987).

[89] Y. Li, W. Guo, L.-C. Du, and D.-C. Mei, Subdiffusion and ergodicity breaking in heterogeneous environments subject to Lévy noise, Physica A **514**, 948 (2019).

[90] X. Wang, W. Deng, and Y. Chen, Ergodic properties of heterogeneous diffusion processes in a potential well, J. Chem. Phys. **150**, 164121 (2019).

[91] T. Sandev, A. Schulz, H. Kantz, and A. Iomin, Heterogeneous diffusion in comb and fractal grid structures, Chaos, Solitons Fractals **114**, 551 (2018).

[92] O. Bénichou, P. Illien, G. Oshanin, A. Sarracino, and R. Voituriez, Diffusion and Subdiffusion of Interacting Particles on Comblike Structures, Phys. Rev. Lett. **115**, 220601 (2015).

[93] M. Heidernätsch, *On the Diffusion in Inhomogeneous Systems*, Ph.D. thesis, TU Chemnitz, 2015.

[94] N. Leibovich and E. Barkai, Infinite ergodic theory for heterogeneous diffusion processes, Phys. Rev. E **99**, 042138 (2019).

[95] Y. Li, R. Mei, Y. Xu, J. Kurths, J. Duan, and R. Metzler, Particle dynamics and transport enhancement in a confined channel with position-dependent diffusivity, New J. Phys. **22**, 053016 (2020).

[96] P. Massignan, A. Lampo, J. Wehr, and M. Lewenstein, Quantum Brownian motion with inhomogeneous damping and diffusion, Phys. Rev. A **91**, 033627 (2015).

[97] A. Donos, J. P. Gauntlett, and V. Ziogas, Diffusion in inhomogeneous media, Phys. Rev. D **96**, 125003 (2017).

[98] C. Gardiner, *Stochastic Methods: A Handbook for the Natural and Social Sciences* (Springer, Berlin, 2009).

[99] N. G. van Kampen, *Stochastic Processes in Physics and Chemistry* (Elsevier, Amsterdam, 1992).

[100] Yu. L. Klimontovich, Nonlinear Brownian motion, Phys. Usp. **37**, 737 (1994).

[101] K. Ito, On stochastic differential equations, Memoirs Amer. Math. Soc. **4**, 51 (1951).

[102] D. L. Fisk, Quasi-martingales, Trans. Am. Math. Soc. **120**, 369 (1965).

[103] R. L. Stratonovich, A new representation for stochastic integrals and equations, J. SIAM Control **4**, 362 (1966).

[104] P. Hänggi, Stochastic processes I: Asymptotic behaviour and symmetries, Helv. Phys. Acta **51**, 183 (1978).

[105] Yu. L. Klimontovich, Ito, Stratonovich and kinetic forms of stochastic equations, Physica A **163**, 515 (1990).

[106] I. M. Sokolov, Ito, Stratonovich, Hänggi and all the rest: The thermodynamics of interpretation, Chem. Phys. **375**, 359 (2010).

[107] O. Farago and N. Grønbech-Jensen, Langevin dynamics in inhomogeneous media: Re-examining the Ito-Stratonovich dilemma, Phys. Rev. E **89**, 013301 (2014).

[108] R. Yuan and P. Ao, Beyond Ito versus Stratonovich, J. Stat. Mech. (2012) P07010.

[109] I. Pavlyukevich and G. Shevchenko, Stratonovich stochastic differential equation with irregular coefficients: Girsanov's example revisited, Bernoulli **26**, 1381 (2020).

[110] G. Volpe, L. Helden, T. Brettschneider, J. Wehr, and C. Bechinger, Influence of Noise on Force Measurements, Phys. Rev. Lett. **104**, 170602 (2010).

[111] W. Koch, A solution of the two-dimensional atmospheric diffusion equation with height-dependent diffusion coefficient including ground level absorption, Atmosph. Envir. **23**, 1729 (1989).

[112] J.-S. Lin and L. M. Hildemann, Analytical solutions of the atmospheric diffusion equation with multiple sources and height-dependent wind speed and eddy diffusivities, Atmosph. Envir. **30**, 239 (1996).

[113] J. Komall, D. Peak, and J. W. Corbett, Impurity-concentration profile for an exponentially decaying diffusion coefficient in irradiation enhanced diffusion, Phys. Rev. B **13**, 477 (1976).

[114] E. W. Maby, Bombardment-enhanced diffusion of arsenic in silicon, J. Appl. Phys. **47**, 830 (1976).

[115] A. G. Kesarev and V. V. Kondratev, On the theory of diffusion in inhomogeneous media: long times of the process, Phys. Metals Metallogr. **108**, 30 (2009).

[116] T. Benesch, S. Yiacoumi, and C. Tsouris, Brownian motion in confinement, Phys. Rev. E **68**, 021401 (2003).

[117] B. Lin, J. Yu, and S. A. Rice, Direct measurements of constrained Brownian motion of an isolated sphere between two walls, Phys. Rev. E **62**, 3909 (2000).

[118] M. Matse, M. V. Chubynsky, and J. Bechhoefer, Test of the diffusing-diffusivity mechanism using near-wall colloidal dynamics, Phys. Rev. E **96**, 042604 (2017).

[119] P. Lancon, G. Batrouni, L. Lobry, and N. Ostrowsky, Drift without flux: Brownian walker with a space-dependent diffusion coefficient, Europhys. Lett. **54**, 28 (2001).

[120] P. Lancon, G. Batrouni, L. Lobry, and N. Ostrowsky, Brownian walker in a confined geometry leading to a space-dependent diffusion coefficient, Physica A **304**, 65 (2002).

[121] G. Dagan, Theory of solute transport by groundwater, Ann. Rev. Fluid Mech. **19**, 183 (1987).

[122] D. L. Koch and J. F. Brady, Anomalous diffusion in heterogeneous porous media, Phys. Fluids **31**, 965 (1988).

[123] P. Gouze, Y. Melean, T. Le Borgne, M. Dentz, and J. Carrera, Non-Fickian dispersion in porous media explained by heterogeneous microscale matrix diffusion, Water Res. Res. **44**, W11416 (2008).

[124] V. M. Goloviznin, P. S. Kondratenko, L. V. Matveev *et al.*, in *Anomalous Radionuclide Diffusion in Highly Heterogeneous Geological Formations*, edited by L. A. Bolshov (Nuclear Safety Institute RAS, Nauka, Moscow, 2010).

[125] T. Kühn, T. O. Ihalainen, J. Hyvaluoma, N. Dross, S. F. Willman, J. Langowski, M. Vihinen-Ranta, and J. Timonen, Protein diffusion in mammalian cell cytoplasm, PLoS ONE **6**, e22962 (2011).

[126] A. Sabri, X. Xu, D. Krapf, and M. Weiss, Elucidating the origin of heterogeneous anomalous diffusion in the cytoplasm of mammalian cells, arXiv:1910.00102.

[127] C. Donth and M. Weiss, Quantitative assessment of the spatial crowding heterogeneity in cellular fluids, Phys. Rev. E **99**, 052415 (2019).

[128] S. K. Ghosh, A. G. Cherstvy, D. S. Grebenkov, and R. Metzler, Anomalous, non-Gaussian tracer diffusion in crowded two-dimensional environments, New J. Phys. **18**, 013027 (2016).

[129] M. Cencini and S. Pigolotti, Energetic funnel facilitates facilitated diffusion, Nucl. Acids Res. **46**, 558 (2018).

[130] X. Chen, X. Cheng, Y. Kang, and J. Duan, Target search of a protein on DNA in the presence of position-dependent bias, J. Stat. Mech. (2019) 033501.

[131] A. Bueno-Orovio, D. Kay, V. Grau, B. Rodriguez, and K. Burrage, Fractional diffusion models of cardiac electrical propagation: Role of structural heterogeneity in dispersion of repolarization, J. R. Soc. Interface **11**, 20140352 (2014).

[132] F. Thiel and I. M. Sokolov, Scaled Brownian motion as a mean-field model for continuous-time random walks, Phys. Rev. E **89**, 012115 (2014).

[133] J. H. P. Schulz, E. Barkai, and R. Metzler, Aging Effects and Population Splitting in Single-Particle Trajectory Averages, Phys. Rev. Lett. **110**, 020602 (2013).

[134] J. H. P. Schulz, E. Barkai, and R. Metzler, Aging Renewal Theory and Application to Random Walks, Phys. Rev. X **4**, 011028 (2014).

[135] H. Safdari, A. V. Chechkin, G. R. Jafari, and R. Metzler, Aging scaled Brownian motion, Phys. Rev. E **91**, 042107 (2015).

[136] M. L. Deng and W. Q. Zhu, Stochastic averaging of quasi-non-integrable Hamiltonian systems under fractional Gaussian noise excitation, Nonlin. Dyn. **83**, 1015 (2016).

[137] F. Biagini, Y. Hu, B. Øksendal, and T. Zhang, in *Stochastic Calculus for Fractional Brownian Motion and Applications*, edited by J. Gani, C. C. Heyde, P. Jagers, and T. G. Kurtz, (Springer-Verlag, London, 2008).

[138] S. C. James nad C. V. Chrysikopoulos, An efficient particle tracking equation with specified spatial step for the solu-

tion of the diffusion equation, Chem. Eng. Sci. **56**, 6535 (2001).

[139] M. Dentz, P. Gouze, A. Russian, J. Dweik, and F. Delay, Diffusion and trapping in heterogeneous media: An inhomogeneous continuous time random walk approach, Adv. Water Resour. **49**, 13 (2012).

[140] A. Russian, *Anomalous Dynamics of Darcy Flow and Diffusion Through Heterogeneous Media*, Ph.D. thesis, Polytechnic University of Catalonia, 2013.

[141] R. Sh. Malkovich, On the analysis of coordinate-dependent diffusion, Techn. Phys. **51**, 283 (2006).

[142] T. Brettschneider, G. Volpe, L. Helden, J. Wehr, and C. Bechinger, Force measurement in the presence of Brownian noise: Equilibrium-distribution method versus drift method, Phys. Rev. E **83**, 041113 (2011).

[143] S. Hottovy, G. Volpe, and J. Wehr, Noise-induced drift in stochastic differential equations with arbitrary friction and diffusion in the Smoluchowski-Kramers limit, J. Stat. Phys. **146**, 762 (2012).

[144] A. G. Kesarev and V. V. Kondratev, To the theory of diffusion in inhomogeneous media: short times of the process, Phys. Metals Metallogr. **106**, 327 (2008).

[145] E. Bringuier, Kinetic theory of inhomogeneous diffusion, Physica A **388**, 2588 (2009).

[146] P. F. Tupper and X. Yang, A paradox of state-dependent diffusion and how to resolve it, Proc. R. Soc. A **468**, 3864 (2012).

[147] O. Farago and N. Grønbech-Jensen, Fluctuation-dissipation relation for systems with spatially varying friction, J. Stat. Phys. **156**, 1093 (2014).

[148] T. Kuroiwa and K. Miyazaki, Brownian motion with multiplicative noises revisited, J. Phys. A **47**, 012001 (2014).

[149] S. Regev, N. Grønbech-Jensen, and O. Farago, Isothermal Langevin dynamics in systems with power-law spatially dependent friction, Phys. Rev. E **94**, 012116 (2016).

[150] M. Wolfson, C. Liepold, B. Lin, and S. A. Rice, A comment on the position dependent diffusion coefficient representation of structural heterogeneity, J. Chem. Phys. **148**, 194901 (2018).

[151] A. Bhattacharyay, Equilibrium stochastic dynamics of a Brownian particle in inhomogeneous space: Derivation of an alternative model, Physica A **494**, 218 (2018).

[152] A. Bhattacharyay, Generalization of Stokes-Einstein relation to coordinate dependent damping and diffusivity: An apparent conflict, J. Phys. A **53**, 075002 (2020).

[153] D. Molina-Garcia, T. Sandev, H. Safdari, G. Pagnini, A. V. Chechkin, and R. Metzler, Crossover from anomalous to normal diffusion: Truncated power-law noise correlations and applications to dynamics in lipid bilayers, New J. Phys. **20**, 103027 (2018).

[154] W. R. Schneider and W. Wyss, Fractional diffusion and wave equations, J. Math. Phys. **30**, 134 (1989)

[155] B. J. West, P. Grigolini, R. Metzler, and T. F. Nonnenmacher, Fractional diffusion and Lévy stable processes, Phys. Rev. E **55**, 99 (1997).

[156] R. Metzler and J. Klafter, Accelerating Brownian motion: A fractional dynamics approach to fast diffusion, Europhys. Lett. **51**, 492 (2000).